Robotics and Computer Integrated Manufacturing 54 (2018) 96–114

Contents lists available at ScienceDirect

Robotics and Computer Integrated Manufacturing

journal homepage: www.elsevier.com/locate/rcim

Trajectory tracking control of a pneumatically actuated 6-DOF Gough–Stewart parallel robot using Backstepping-Sliding Mode controller and geometry-based quasi forward kinematic method

Amir Salimi Lafmejani[a,b], Mehdi Tale Masouleh[*,a,c], Ahmad Kalhor[a,c]

[a] Human and Robot Interaction Laboratory, School of Electrical and Computer Engineering, University of Tehran, North Kargar Street, Iran
[b] Faculty of New Sciences and Technologies, University of Tehran, Iran
[c] School of Electrical and Computer Engineering, University of Tehran, North Kargar Street, Iran

ARTICLE INFO

Keywords:
Trajectory tracking
Gough–Stewart platform
Backstepping-Sliding Mode controller
Forward kinematic problem
Pneumatic actuator

ABSTRACT

In this paper, the trajectory tracking control of a 6-DoF pneumatically actuated Gough–Stewart parallel robot is investigated. The dynamic model of each link, comprising of a pneumatic actuator and a proportional electrical valve is extracted with the aim of obtaining the corresponding state space representation of the pneumatic system. Unknown parameters of the dynamic model consisting friction force of the cylinder and parameters of the proportional valve are identified by employing genetic algorithm. Position control of the pneumatic actuator is performed based on Back-Stepping Sliding Mode controller according to the dynamic model of the system. As such trajectory tracking control is performed for different trajectories by employing a rotation sensor and calculated position based on joint space and task space simultaneously. Desired sinusoidal trajectories with pure motions are tracked with root mean square error of the pure translations and rotations lower than 0.85 (cm) and 1.9 (deg), respectively. The results reveal that the trajectory is tracked by the Back-Stepping Sliding Mode controller properly. This shows the efficiency of the control strategy and the proposed method for calculating the position of the end-effector.

1. Introduction

Parallel robots entail many advantages compared to their counterparts, serial robots, such as higher rigidity, higher load-to-weight ratio, higher precision and can reach to a higher speed and acceleration [1]. The Gough–Stewart Platform (GSP) a 6 °-of-freedom (6-DoF) parallel robot has a movable platform, called End-Effector (E-E), connected to a fixed base platform via 6 expandable actuators [2]. The GSP is used in various applications and manufacturing, e.g., flight simulators and aeronautics applications [3], radio telescopes [4], tire test machines [5], multi-dimensional vibration isolation mechanisms [6] and rehabilitation [7,8].

Trajectory tracking is one of the challenging problems in manufacturing for this kind of parallel robot according to its complicated dynamic and kinematic modeling [9,10]. Two strategies have been proposed to control a GSP, namely joint space control and task space control. In [11], the joint space control has been developed by measuring desired lengths of the GSP's actuators, which has been obtained based on solving the inverse kinematic problem of the desired trajectory in task space. Although, the task space control is more precise and it is more complicated than the joint space control. Task space control can be performed based on: (1) Position and rotation of the GSP's E-E using vision, position and orientation sensors [12], (2) Solving forward kinematic problem (FKP) using the measured lengths of the GSP's links [13]. The first approach might be very expensive and the latter method deals with computational effort. In [14], a vision-based control has been investigated for control of a 6-DoF parallel robot in which the pose of E-E was measured by a motion-tracking system. In the foregoing study, a H_∞ controller is implemented in order to tune the control signal. In [15], a novel method has been proposed for solving nonlinear equations in FKP of a parallel robot based on Homotopy Continuation method. Their method has been implemented in solving FKP of a 3-RPR parallel robot with high precision in results. Moreover, a real-time solution for solving froward kinematic problem of a GSP has been proposed in [16]. In [17], a comparative study has been investigated in differences between the results of conventional and the proposed methods.

Complexity or simplicity of the trajectory tracking problem depends on the type of actuators. There are three types of actuators for driving a GSP which are electric, hydraulic and pneumatic. Using a pneumatic

* Corresponding author at: Human and Robot Interaction Laboratory, School of Electrical and Computer Engineering, University of Tehran, North Kargar Street, Iran.
E-mail address: m.t.masouleh@ut.ac.ir (M. Tale Masouleh).

https://doi.org/10.1016/j.rcim.2018.06.001
Received 3 May 2017; Received in revised form 4 June 2018; Accepted 9 June 2018
Available online 27 June 2018
0736-5845/ © 2018 Elsevier Ltd. All rights reserved.

actuator has some drawbacks which mainly originate from compressibility of the air, different regimes of air flow through valves, and dynamic behavior of friction force of a pneumatic cylinder. On the other hand, it has many advantages in comparison with other types of driving systems, such as a cost-effective actuation, clean for the working environment, easy to maintenance, and rapid movement and reactions.

Different control strategies have been developed by researchers in control of a 6-DoF GSP such as LQG controller, PID controller, Robust approaches, Adaptive control strategy, and Sliding-Mode controller. In [18], the Linear Quadratic Gaussian (LQG) controller based on reference tracking has been designed for motion control of a pneumatically-driven 6-DoF GSP. The LQG controller has been designed by combining a Linear Quadratic Estimator (LQE) with a Linear Quadratic Regulator (LQR). In the foregoing study, the authors evaluated the robustness of the control under different external loads in experimental tests. In [19], the PID controller with feedback linearization have been designed for trajectory tracking of a 6-DoF pneumatically GSP. In the foregoing study, the authors preferred using heuristic algorithm to solve the non-convex problems for tuning the controller's parameters. The inner control loop has been used for controlling the work pressure and the outer loop has been related to displacement of the load under various external forces. Their analysis was performed in the Simulink of the MatLab software. In [20], a pneumatic wearable walking assistance GSP has been developed for ankle-foot rehabilitation system. Double-acting pneumatic actuators have been used and an I-PD controller has been designed to control the platform at a desired position. They proved that overshoot of an I-PD controller is smaller than usual PID controller.

In [21], an adaptive controller has been proposed for the position tracking of a 6-DoF SGP driving simulator in numerical simulation based on a linearized dynamic equations model. The authors have employed two inner and outer control loops and the combined PD controller and adaptive compensation has been applied for the control design. In [22], a robust adaptive controller of a 6-DoF parallel robot has been investigated without requiring inverse dynamic model. Besides, they used a hybrid method based on Sliding Mode and Neural Networks in order to control the robot. In [23], an experimental study on an accurate model-based controller of a 6-DoF parallel robot has been carried out in order to improve the tracking accuracy in both joint and task spaces. Robust control design has been applied for a single actuator developed by a feed-forward dynamic compensator and a feedback-observer controller. In [24], a robust adaptive controller has been proposed based on task space dynamic equations. To this end, a 6-DoF GSP was built in Simulink environment of MatLab software. The authors evaluated performance of the proposed controller for sinusoidal trajectory tracking. Sliding Mode control strategy has the potential to be used for control of robotic systems with large uncertainties [25]. In [26], a simulation-based study has been investigated in position control of a typical SGP based on smooth integral sliding mode controller. The discontinuous controller has been replaced by a twisting algorithm based on combination of two continuous controls. Their method is robust to external matched disturbances of the system. Moreover, vision-based methods have been widely explored in the literature for controlling parallel robots. In [27], a visual-based kinematic model of a GSP has been investigated through the observation of its legs which has been inspired by geometry of lines. They claimed that the proposed method simplified both identification and control of the GSP. In [28], a general concept of visual servoing of parallel robots has been proposed which is based on hidden robot model based on observing the leg directions.

The main contribution of this paper is proposing a closed-loop control strategy for a 6-DoF pneumatically actuated Gough-Stewart platform, namely HexaTaar, with the aim of solving the trajectory tracking problem. The HexaTaar is actuated by 6 pneumatic systems (PneuSys) which each of them consists a proportional directional electrical valve and a pneumatic actuator. The unknown parameters of the PneuSys including mass flow rate through the proportional valve, viscosity coefficient and friction force of the pneumatic actuator are identified based on evolutionary algorithm, the so-called Genetic Algorithm (GA). The PneuSys are considered independent and the effects of other actuators on each one are considered as an external disturbance and uncertainties. Therefore, the identified PneuSys is controlled by employing Backstepping-Sliding Mode controller, separately. In this paper, the trajectory tracking control is performed based on combination of the joint space and task space control, simultaneously. Moreover, a novel approach is proposed, namely Geometry-based Quasi Forward Kinematic (GQFK) method, in order to calculate the position of the HexaTaar's E-E without using position sensors and vision-based observations. In the GQFK method, position of the E-E along the x, y and z axes are calculated using the angles measured by the IMU sensor and the potentiometers.

The remainder of this paper is organized as follows. The experimental setup of the 6-DoF pneumatically actuated robot and mechanical parts are described in Section 2. Moreover, mathematical model of the PneuSys including cylinder and pressure dynamic with the aim of obtaining the state space representation of the PneuSys are extracted. Section 3 is devoted to identification procedure of the PneuSys's unknown parameters using GA, and the proposed controller, BS-SMC, is designed for position control of the pneumatic actuator. The proposed closed-loop control strategy including outer and inner control loops for trajectory tracking control of the HexaTaar robot using the nonlinear controller BS-SMC and GQFK method are explained in Section 4. Finally, the paper concludes with some hints and remarks as ongoing works.

2. Experimental setup of the 6-Dof hexataar parallel robot

In this section, geometry configuration and size of different mechanical parts of the HexaTaar robot are introduced. Moreover, the PneuSys of each link of the robot is explained in details.

2.1. The 6-dof hexataar robot's configuration

Fig. 1 demonstrates the under study 6-UPS GSP robot, which has been constructed at Human and Robot Interaction Laboratory (TaarLab). As aforementioned, this robot consists of a fixed base, six pneumatically actuated links, and a moving platform (E-E). The HexaTaar is categorized as a 6-6 GSP pneumatically driven parallel robot. Fig. 2exhibits the explosion configuration of the HexaTaar robot. According to Fig. 2, Table 1 describes all of the numbered HexaTaar's components.

2.2. The pneumatic system

The 6-DoF HexaTaar robot has six PneuSys in which a pneumatic actuator plays an actuating role in the robot. Fig. 3 exhibits the experimental PneuSys of each link of the HexaTaar robot in which the PneuSys includes a proportional directional electrical valve, a pneumatic actuator, mechanical guide, a potentiometer and two pressure sensors. The proportional electrical valve guides the air flow through chambers of the pneumatic actuator according to the spool position which depends on the input command voltage of the valve. Pressure of the actuator's chambers are obtained by pressure sensors which are placed in the way of air flow. On the other hand, pneumatic force enables the actuator to have upward and downward strokes with different velocities to make various pose for the moving platform. The position of the cylinder can be calculated by means of variable resistor in the potentiometer sensor and the derivative of the cylinder displacement results in its velocity. Besides, mechanical guide improve stiffness of the pneumatic actuator during different motions of the HexaTaar robot. Fig. 5 shows the experimental electro-pneumatic setup of the pneumatic

Fig. 1. The pneumatically actuated 6-DoF UPS HexaTaar robot based on 6-6 Gough-Stewart Platform, constructed in Human and Robot Interaction Laboratory, University of Tehran.

system, including pneumatic actuator, directional proportional electrical valve, which is equipped with three pressure sensors and linear displacement encode (potentiometer) as position feedback sensor.

2.2.1. Mathematical model of the pneusys

In this section, mathematical dynamic model of the PneuSys of the HexaTaar is extracted to obtain the state space representation of the nonlinear system. To do so, the nonlinear dynamic equations of the pneumatic cylinder and proportional electrical valve should be derived. The mathematical model of the PneuSys including pneumatic actuator and proportional control valve has been investigated in [17]. For the sake of clarity and quick reference, the nomenclatures which are used in the foregoing mathematical model are listed in Table 2.

2.2.2. Cylinder dynamics

Fig. 4, demonstrates free body diagram of the pneumatic cylinder

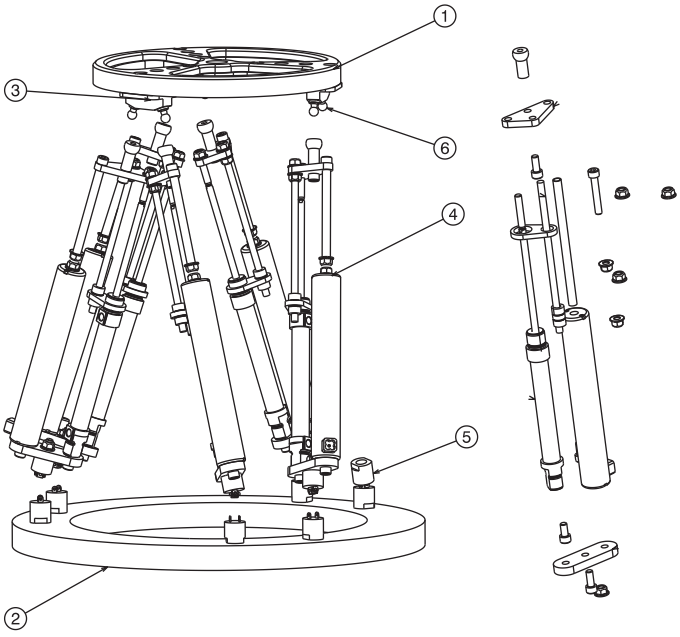

Fig. 2. Explosion plan of the 6-DoF UPS HexaTaar robot.

Table 1
The characteristics of the explosion configuration of the 6-DoF HexaTaar robot.

Number	Description
1	E-E of the HexaTaar
2	Fixed base of the HexaTaar
3	Connecting point of the links to the E-E
4	Link of the HexaTaar consisting pneumatic actuator
5	Universal joint connected to fixed base of the HexaTaar
6	Spherical joint connected to E-E of the HexaTaar

which consists of weight, friction and pneumatic forces. Dynamic equations of the pneumatic cylinder are obtained from the second Newton's law for upward strokes in Eq. (1), and downward strokes in Eq. (2) as follows:

$$Ma = P_1A_1 - P_2A_2 - P_aA_r - Mg - F_f \tag{1}$$

$$Ma = P_1A_1 - P_2A_2 - P_aA_r - Mg + F_f \tag{2}$$

where F_f is modeled based on a prominent friction model, the so-called LuGre model. The LuGre model of friction force was introduced in [29,30], as a function of cylinder velocity, stribeck velocity, static and coulomb friction forces. Based on the latter studies, the friction model can be expressed mathematically as:

$$F_f = F_c\text{sgn}(v) + (F_s - F_c)\exp\left(-\left(\frac{v}{v_s}\right)^2\right)\text{sgn}(v) + Bv \tag{3}$$

Moreover, stribeck velocity [31], v_s, viscous coefficient B, static friction, F_s, and coulomb friction, F_c, are unknown parameters which should be identified and then substituted into the dynamic model based on Eqs. (1)and (2). In [32], the unknown parameters of dynamic model of a 3-DoF decoupled robot have been identified based on experimental tests and using evolutionary algorithm.

2.2.3. Pressure dynamics

According to [17], a model for the mass flow rate of a compressible air through chambers of the cylinder was proposed as follows:

Table 2
Nomenclatures used in expressing the mathematical model of the PneuSys.

Parameter's description	Symbol	Dimension
Atmosphere pressure	P_a	N/m^2
Chamber i area	A_i	m^2
Chamber i pressure	P_i	N/m^2
Coulomb friction	F_c	N
Critical pressure	P_c	N/m^2
Cylinder acceleration	a	m/s^2
Cylinder velocity	v	m/s
Discharge coefficient	C_d	–
Downstream pressure	P_d	N/m^2
Friction force	F_f	N
Gravitational coefficient	g	m/s^2
Inactive volume	V_0	m^3
Inlet mass flow rate	$\dot{m}_i$	N/m^2
Input voltage	u	V
Load position	x	m
Outlet mass flow rate	$\dot{m}_o$	N/m^2
Piston mass	M	kg
Rod area	A_r	m^2
Specific heat constant	k	–
Spool displacement	X_{spool}	m
Static friction	F_s	N
Stroke length	L	m
Stribeck velocity	v_s	m/s
Supply pressure	P_s	N/m^2
Temperature	T_s	K
Universal gas constant	R	J/K.kg
Upstream pressure	P_u	N/m^2
Valve constants	C_v	–
Valve orifice area	A_v	m^2
Viscous coefficient	B	N.s/m
Volume of ith chamber	V_i	m^3

$$\dot{m}(P_u, P_d) = \begin{cases} C_f A_v \left(\frac{k}{R}\frac{2}{k-1}\right)^{\frac{1}{2}} \frac{P_u}{\sqrt{T}} \left(\frac{P_d}{P_u}\right)^{\frac{1}{k}} \left(1 - \left(\frac{P_d}{P_u}\right)^{\frac{k-1}{k}}\right)^{\frac{1}{2}}, & \frac{P_d}{P_u} > P_c \\ C_f A_v \frac{P_u}{\sqrt{T}} \left(\frac{k}{R}\left(\frac{2}{k+1}\right)^{\frac{k+1}{k-1}}\right)^{\frac{1}{2}}, & \frac{P_d}{P_u} < P_c \end{cases} \tag{4}$$

Furthermore, the critical pressure, P_c is determined by,

$$P_c = \left(\frac{2}{k+1}\right)^{\frac{k}{k-1}} \tag{5}$$

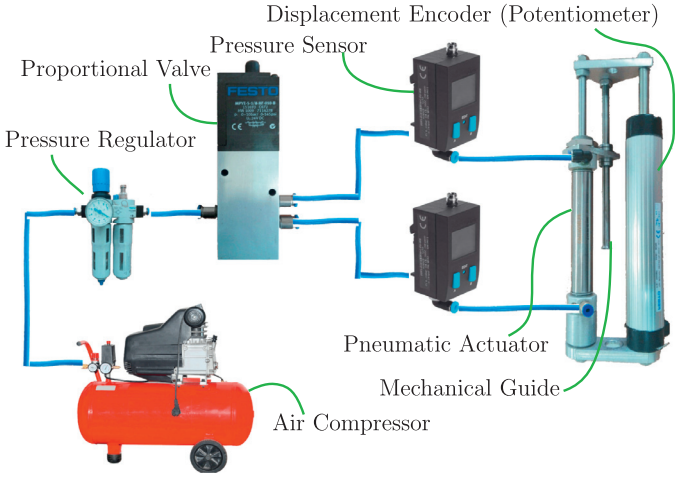

Fig. 3. The experimental setup of each PneuSys of the links which consists of a pneumatic actuator, a directional proportional electrical valve, two pressure sensors and a linear displacement encoder (potentiometer).

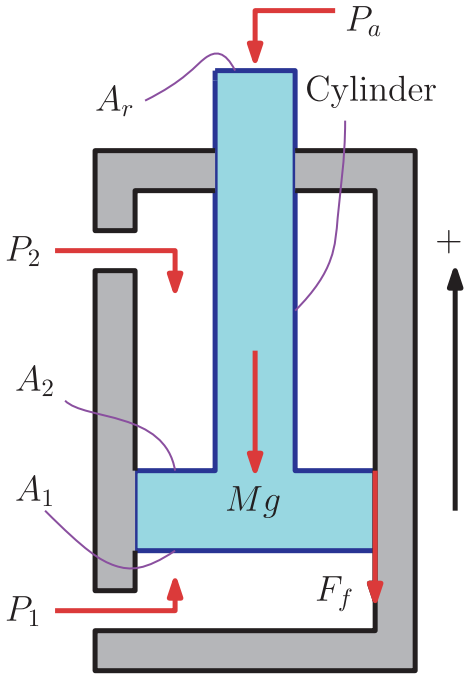

Fig. 4. Free body diagram of the pneumatic actuator's cylinder.

According to the standard ISO–6358, specific heat ratio, gas constant, temperature and atmosphere pressure have been determined based on the environment conditions of the experiment which are listed in Table 3. Thus, by substituting value of k in Eq. (5), P_c will be 0.528. The relationship between spool displacement and input command voltage described in [33], is calculated as follows:

$$A_v = \pi \frac{X_{\text{spool}}^2}{4}, \quad X_{\text{spool}} = C_v u$$
$$\dot{m} \propto A_v \propto X_{\text{spool}}^2 \propto u^2 \tag{6}$$

where effective area of the proportional valve, A_v, is $15 \times 10^{-6}(\text{m}^2)$ and C_v is an intrinsic and unknown nonlinear parameter of the valve. The

Table 3
Constant parameters of the environment conditions of the experiment place.

Symbol	Value	Dimension
k	1.4	–
T	294	K
R	287	J/K.kg
P_a	10^5	N/m^2

Table 4
Relative pressure for the upward strokes.

Chamber	Upstream	Downstream
Chamber 1	P_s	P_1
Chamber 2	P_2	P_a

Table 5
Relative pressure for the downward strokes.

Chamber	Upstream	Downstream
Chamber 1	P_1	P_a
Chamber 2	P_s	P_2

upstream and downstream are different for upward and downward strokes. Tables 4 and 5 represent the upstream and downstream pressures at each conditions for the upward and downward strokes, respectively. Finally, the dynamic equations of the PneuSys are obtained by Eqs. (1) and (2). Referring to [34] where by considering the changes of heat ratio in the cylinder, one has:

$$\begin{aligned} a &= \frac{1}{M}(P_1 A_1 - P_2 A_2 - P_a A_r - Mg \mp F_f) \\ \dot{P}_1 &= \frac{RT}{V_1}(\gamma_i \dot{m}_{i,1} - \gamma_o \dot{m}_{o,1}) - \gamma_k \left(\frac{P_1}{V_1}\right)\dot{V}_1 \\ \dot{P}_2 &= \frac{RT}{V_2}(\gamma_i \dot{m}_{i,2} - \gamma_o \dot{m}_{o,2}) + \gamma_k \left(\frac{P_2}{V_2}\right)\dot{V}_2 \end{aligned} \tag{7}$$

In the above, $\dot{P}_1$ and $\dot{P}_2$ stand for the pressure dynamics in the chambers

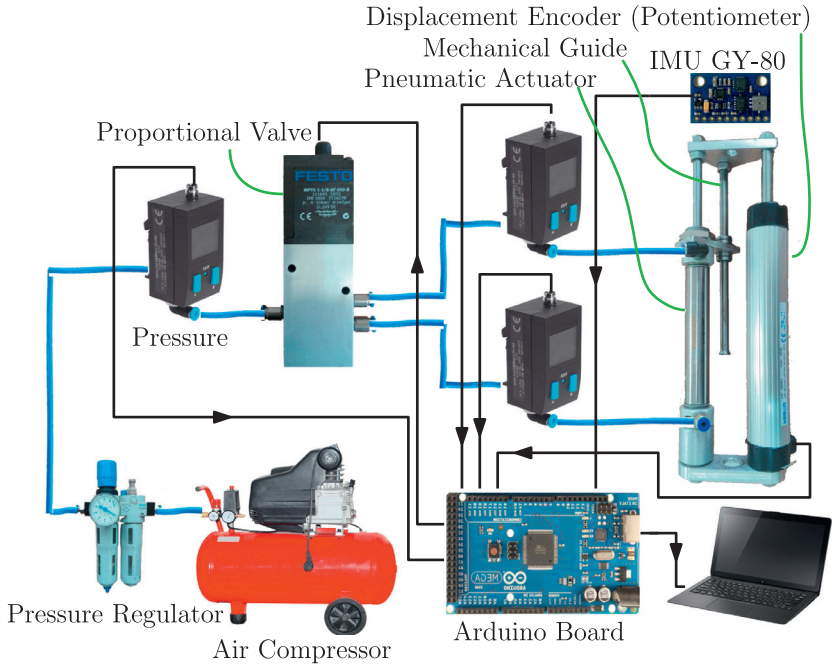

Fig. 5. The experimental setup of the PneuSys consisting pneumatic and electrical circuits and sensors.

of the cylinder. The piston dynamics in the first equation of Eq. 7 is obtained based on Eqs. (1) and (2). Moreover, the details of obtaining the dynamic equations of the proportional valve, which are the second and third equations in Eq. (7), are explained in Appendix 1.

2.2.4. State space representation of the pneusys

Assume that $x_1 = x$, $x_2 = v$, $x_3 = P_1$ and $x_4 = P_2$. By considering the aforementioned equations, and the load and pressure dynamics and upon rewriting Eq. (7), the state space representation of the PneuSys consists in dynamic equations of pneumatic actuator and proportional directional control valve are as follows:

$$\begin{aligned}
\dot{x}_1 &= x_2 \\
\dot{x}_2 &= \frac{1}{M}(x_3 A_1 - x_4 A_2 - P_a A_r - Mg \mp F_f) \\
\dot{x}_3 &= \frac{RT}{V_1}(\gamma_i \dot{m}_{i,1} - \gamma_o \dot{m}_{o,1}) - \gamma_k \left(\frac{x_3}{V_1}\right)\dot{V}_1 \\
\dot{x}_4 &= \frac{RT}{V_2}(\gamma_i \dot{m}_{i,2} - \gamma_o \dot{m}_{o,2}) + \gamma_k \left(\frac{x_4}{V_2}\right)\dot{V}_2
\end{aligned} \tag{8}$$

where the sign of double-signed F_f is determined based on the stroke whether velocity of the cylinder is positive or negative. The upper sign is related to the positive velocity or upward strokes and the lower sign refers to the negative velocity or downward strokes.

In practice, position of the cylinder, x_1, which is obtained by a real-time manner, is observed by potentiometer sensor and x_2 stands for the velocity which is the derivative of the displacement of the piston. A gaussian filter is employed to remove possible noise on the velocity, which is originated from derivation procedure, and leads to have a smooth velocity data. Furthermore, P_1 and P_2 are observed by pressure sensors.

3. Identification of the pneusys and position control of the pneumatic actuator

The obtained dynamic model in Section 2.2.1 has unknown parameters, e.g., friction force and viscose coefficient of the pneumatic actuator, mass flow rate through the proportional valve. In this section, the unknown parameters of the PneuSys is identified according to the extracted dynamic model in Eq. (8). Moreover, position control of the pneumatic actuator is performed by designing a nonlinear controller, namely Backstepping-Sliding Mode controller.

The PneuSys of each link of the robot which has been demonstrated in Fig. 3 should be equipped with an extra pressure sensor and accelerometer sensors for identification and control procedures. The detailed specification of all components are listed in Table 6. The extra pressure sensor is connected between the supply pressure and the inlet port of the proportional valve which measures the supply pressure, P_s. Moreover, the accelerometer sensor is fixed at the end of the cylinder of the pneumatic actuator in order to measure acceleration of the cylinder, a. The pressure regulator adjusts supply pressure of the pneumatic system which is measured by the pressure sensor connected to the input port of the electrical valve. The potentiometer sensor measured the displacement of the pneumatic cylinder and the derivative of the piston displacement results in its velocity. Moreover, linear acceleration of the cylinder is computed by an accelerometer sensor ADXL345 and an angular acceleration which is received by a gyro sensor L3G4200D in IMU-GY80. The linear acceleration and gyroscope data are calculated using data fusion process available in Arduino codes which leads to achieve accurate value of linear acceleration along the *X, Y* and *Z* coordinate axes during the aforementioned strokes [35].

Table 6
Specifications of the electro-pneumatic experimental setup components.

Component	Model	Manufac.
Actuator	DSNU-20-100-PPV-A	FESTO
Electrical valve	MPYE-5-1/8-HF-010-B	FESTO
Position sensor	MLO-POT-100-LWG	FESTO
Pressure sensor	SED1-D10-G2-H18	FESTO
Pressure regulator	LFR-D-MINI	FESTO
Accelerometer	IMU GY-80	Sparkfun

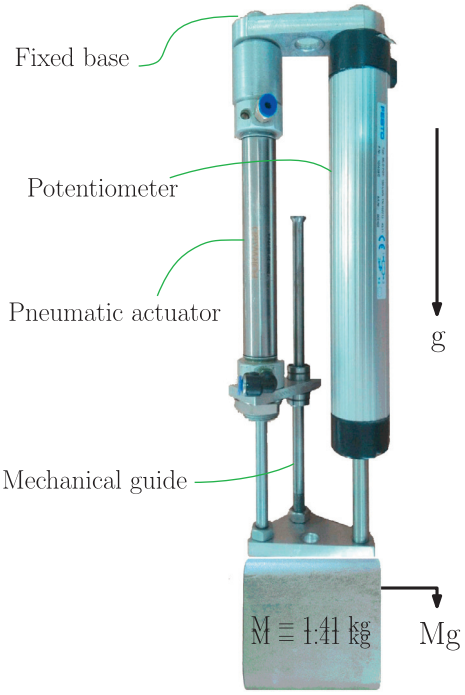

Fig. 6. The setup for performing the Free-Fall test in order to obtain the viscous coefficient and the Coulomb friction.

3.1. Identification of unknown parameters in dynamic model of the pneusys

As depicted in Fig. 5, the linear acceleration and gyroscope data are calculated and using data fusion process available in Arduino codes the accurate value of linear acceleration along the z coordinate axis during the upward and downward strokes is computed.

The viscous coefficient can be computed based on an experimental test, called Free-Fall test. Referring to [17], the viscous coefficient is calculated in such a way that pneumatic force is not exerted which is based on the so-called Free-Fall test [36]. By solving a second order differential equation of cylinder dynamics, viscous coefficient and Coulomb friction are obtained. As shown in Fig. 6, the pneumatic actuator which is coupled mechanically with guide and potentiometer sensor, are fixed to the base and have been hanged on reversely. The pneumatic actuator falls freely with a 1.410kg external load which was hanged from the cylinder.

The weight of the piston has been taken into account in the Free-Fall test. Since the pneumatic force is not exerted in the test, zero-valued parameters, P_s, P_1 and P_2 in Eq. (1) can be eliminated. In Fig. 6 the positive direction of forces is downward. Thus, the resulted equation is obtained as following:

$$\begin{aligned}
&a = \ddot{x}, \quad v = \dot{x}, \quad M = M_{\text{Load}} + M_{\text{p}} \\
&M\ddot{x} = Mg - P_{\text{atm}} A_{\text{rod}} - F_{\text{fric}} - B\dot{x} \\
&\ddot{x} = g - \frac{P_{\text{atm}} A_{\text{rod}}}{M_{\text{load}} + M_{\text{p}}} - \frac{F_{\text{fric}}}{M_{\text{load}} + M_{\text{p}}} - \frac{B\dot{x}}{M_{\text{load}} + M_{\text{p}}}
\end{aligned} \tag{9}$$

where M_{load}, M_{p}, and F_{fric} are mass of the load, mass of the piston, and Coulomb friction, respectively. The term $P_{\text{atm}} A_{\text{rod}}/(M_{\text{load}} + M_{\text{p}})$, which has a constant small value, can be ignored as compared to other terms in Eq. (9). Thus, the differential equation of the load dynamics is,

$$\ddot{x} = g - \frac{g}{W}F_{\text{fric}} - \frac{g}{W}B\dot{x} \tag{10}$$

where $W = (M_{\text{Load}} + M_{\text{p}})g$ is the total weight of load and piston of the actuator. Assume the boundary values as initial conditions for the actuator dynamic $x = 0$ and $\dot{x} = 0$, accordingly. Referring to [36], by solving the second order differential equation in Eq. (10), Coulomb friction and viscous coefficient can be expressed as:

$$F_{\text{fric}} = W\left(1 - \frac{c_1}{gc_2}\right) \tag{11}$$

$$B = \frac{W - F_{\text{fric}}}{c_1} \tag{12}$$

where c_1 and c_2 are constant parameters. The values of the constants are calculated by minimizing RMS error corresponding to the experimental results of x and exponential model. The formulations of obtaining the Coulomb friction and viscous coefficient are explained in details in Appendix 2. Finally, the Coulomb friction and viscous coefficient, obtained by the Free-Fall test, are found to be 73.183(N) and 1.539(N.s/m), respectively.

For the purpose of this study, Genetic Algorithm (GA) is applied in order to obtain the unknown parameters. The GA is employed to find values for the unknown parameters, aiming at minimizing the errors of acceleration, the time derivative of pressure 1, and the time derivative of pressure 2 in the left side of Eq. (8). The errors are originated from substituting the suggested values by GA in the right side of Eq. (8). The objective function in the GA optimization procedure is based on the Normalized Root Mean Square Error (NRMSE) criterion:

$$Z = \sqrt{\frac{1}{n}\sum_{i=2}^{4}\left(\frac{e_i}{\dot{x}_{i,\text{range}}}\right)^2} \tag{13}$$

where e_i indicates the aforementioned error of ith equation for the corresponding suggested solution by GA. The $\dot{x}_{i,\text{range}}$ is the feasible range of the variables $\dot{x}_2$, $\dot{x}_3$, and $\dot{x}_4$ in Eq. (8). The value for the variables' maximum and minimum are obtained through experimental tests in which the pneumatic actuator is forced to work at its maximum and minimum velocity, corresponding to lower and upper range for the input voltage of the proportional valve for the upward and downward strokes of the actuator.

In applying the evolutionary-based identification approach, without loosing the generality, it has been assumed that the viscous coefficient has a constant value which is calculated by the Free-Fall test. The GA parameters for identification of the unknown variables are included in Table 7. The number of variables is determined according to the number of unknown parameters. All the solutions are proposed by GA in the range of [0 1], or between the minimum of variables (VarMin) and maximum of variables (VarMax) for each unknown variable. According to different range of variations of the variables, the proposed solutions between 0 and 1 are mapped to the corresponding feasible range of them, which are predefined in the MatLab program. Furthermore, the stop condition of the GA is based on the value of maximum iteration (MaxIt). Number of population (nPop) is adjusted to the value by which the GA achieve to optimal solutions in a short time. The proposed solutions are normalized according to their feasible ranges.

Table 7
GA parameters for identification of the unknown parameters.

Parameter	Value	Description
nVar	7	number of variables
VarMin	0	minimum of variables
VarMax	1	maximum of variables
MaxIt	1000	maximum iteration
nPop	100	number of populations
pc	0.8	crossover percentage
pm	0.3	mutation percentage
mu	0.02	mutation rate

Table 8
The identified parameters of the dynamic equations of the PneuSys using GA method.

Parameter	Dimension	Up. stroke	Down. stroke
v_s	m/s	0.5641	−0.2894
B	N.s/m	34.4445	−3.2342
F_s	N	86.6540	−91.9421
F_c	N	49.1371	−78.8793
γ_o	–	1.045	1.029
γ_i	–	1.364	1.341
γ_k	–	1.172	1.651

The friction force is modeled according to the positive and negative velocity which are related to the upward and downward strokes, respectively. Furthermore, three parameters γ_o, γ_i and γ_k for pressure dynamic equations are identified based on the evolutionary method. Eventually, the unknown parameters are calculated according to the obtained experimental data, gathered from the potentiometer and pressure sensors, so that the dynamical equations of the PneuSys should be satisfied. The identification of unknown parameters of dynamic equations of the PneuSys which is based on the experimental tests are listed in Table 8.

3.2. Position control of the pneumatic actuator using Backstepping-Sliding Mode controller

Referring to Eq. (8), the state space representation of the Backstepping-Sliding Mode controller is proposed for the trajectory tracking purpose of the nonlinear PneuSys setup. By taking into account the state space of the PneuSys according to Eq. (8), the state space equations include 4 state variables, $X = [x \quad v \quad P_1 \quad P_2]$, which stands for the position, velocity, pressure dynamics of chambers 1 and 2, respectively. By rewriting Eq. (7) and defining C as follows:

$$C = -P_a A_r - Mg - \left[F_c \text{sgn}(x_2) + (F_s - F_c)e^{-\left(\frac{x_2}{v_s}\right)^2}\text{sgn}(x_2)\right] \tag{14}$$

where C indicates constant terms of the load dynamic equation. Thus, it leads to have $\ddot{x}$ as follows:

$$\begin{aligned} \dot{x}_1 &= x_2 \\ \dot{x}_2 &= x_3 A_1 - x_4 A_2 - Bx_2 + C \\ \dot{x}_3 &= F_1(X, u) \\ \dot{x}_4 &= F_2(X, u) \\ y &= x_1 \end{aligned} \tag{15}$$

Assume that ϕ consists of state variables corresponding to dynamic equations of proportional valve, x_3 and x_4. Thus ϕ can be obtained by,

$$\phi = x_3 A_1 - x_4 A_2 \tag{16}$$

Eventually, load dynamic equations are as follows:

$$\begin{aligned} \dot{x}_1 &= x_2 \\ \dot{x}_2 &= \phi - Bx_2 + C \end{aligned} \tag{17}$$

Thus one has,

$$\ddot{x}_1 = \phi - B\dot{x}_1 + C \tag{18}$$

For the sake of applying the concept of SMC, the sliding surface is defined as follows,

$$\begin{aligned} S &= (\dot{x}_1 - \dot{x}_{d,1}) + \lambda(x_1 - x_{d,1}) \\ &= \dot{e}_x + \lambda e_x \end{aligned} \tag{19}$$

where e_x and $\dot{e}_x$ indicate the position error and variation of position error, respectively. The derivative of sliding surface with respect to the time can be calculated as follows:

$$\begin{aligned}\dot{S} &= \ddot{e}_x + \lambda\dot{e}_x \\ &= \ddot{x}_1 - \ddot{x}_{d,1} + \lambda\dot{e}_x \\ &= \phi - B\dot{x}_1 + C - \ddot{x}_{d,1} + \lambda\dot{e}_x\end{aligned} \tag{20}$$

Assuming that C and B are unknown parameters which are estimated by $\hat{C}$ and $\hat{B}$, respectively. Thus, it can be assumed that:

$$\begin{aligned}|C-\hat{C}| &< \overline{C} \\ |B-\hat{B}| &< \overline{B}\end{aligned} \tag{21}$$

By considering ϕ,

$$\phi = \hat{\phi} - K\text{sgn}(S) \tag{22}$$

where $K > 0$, which results in the following for $\hat{\phi}$,

$$\hat{\phi} = arg_{\phi}\left(\dot{S} = 0|_{B=\hat{B},C=\hat{C}}\right) \tag{23}$$

By rewriting Eq. (20), one has:

$$\hat{\phi} - \hat{B}\dot{x}_1 + \hat{C} - \ddot{x}_{1,d} + \lambda\dot{e}_x = 0 \tag{24}$$

Finally, $\hat{\phi}$ can be expressed as follows:

$$\hat{\phi} = \hat{B}\dot{x}_1 - \hat{C} + \ddot{x}_{1,d} - \lambda\dot{e}_x \tag{25}$$

By substituting $\hat{\phi}$ into Eq. (22):

$$\phi = \hat{B}\dot{x}_1 - \hat{C} + \ddot{x}_d - \lambda\dot{e}_x - K\text{sgn}(S) \tag{26}$$

Lyaponov function is defined as follows:

$$V_s = \frac{1}{2}S^2 \tag{27}$$

By calculating the derivative of V_s with respect to the time, one has:

$$\begin{aligned}\dot{V}_s &= S\dot{S} \\ &= S(\phi - B\dot{x}_1 + C - \ddot{x}_{1,d} + \lambda\dot{e}_x) \\ &= S(\hat{B}\dot{x}_1 - \hat{C} - B\dot{x}_1 - K\text{sgn}(S) + C) \\ &= S((\hat{B} - B)\dot{x}_1 + (C - \hat{C}) - K\text{sgn}(S))\end{aligned} \tag{28}$$

Finally, $\dot{V}$ can be summarized as follows:

$$\dot{V} = S(\hat{B} - B)\dot{x}_1 + (C - \hat{C})S - K|S| \tag{29}$$

According to Eq. (21), K is defined as follows:

$$K = \eta + \overline{B}\gamma_{\dot{x}} + \overline{C}, \quad \eta > 0 \tag{30}$$

According to the so-called Schwartz inequality and referring to Eq. (21) it can be concluded that:

$$\begin{aligned}S(\hat{B} - B)\dot{x}_1 &\le |S||B - \hat{B}||\dot{x}_1| \le |S|\overline{B}\gamma_{\dot{x}} \\ S(C - \hat{C}) &\le |S||C - \hat{C}| \le |S|\overline{C}\end{aligned} \tag{31}$$

where $\gamma_{\dot{x}}$ is the upper bound of the following term:

$$A_1F_1(X, u) - A_2F_2(X, u) = -\gamma_{\dot{x}}|\dot{x}| \tag{32}$$

Thus, $\dot{V}$ can be expressed as follows,

$$\dot{V} \le (\overline{B}\gamma_{\dot{x}} + \overline{C} - K)|S| \tag{33}$$

Thus,

$$\dot{V}_s \le -\eta|S| \tag{34}$$

As a result, S converges to zero in a limited time T where $T \le \frac{1}{\eta}$.

By defining z according to the following:

$$z = x_3A_1 - x_4A_2 - \phi \tag{35}$$

Lyaponov function for the main state space system is defined as follows:

$$W = V_s + \frac{1}{2}z^2 \tag{36}$$

By derivating the Lyaponov function with respect to the time one has:

$$\begin{aligned}\dot{W} &= S\dot{S} + z\dot{z} \\ &= S((\hat{B} - B)\dot{x}_1 + (C - \hat{C}) - K \times \text{sgn}(S)) + z(A_1F_1(X, u) - A_2F_2(X, u) - \dot{\phi})\end{aligned} \tag{37}$$

Finally, it leads to the following equation in which the control strategy can be computed once it is solved for u:

$$(A_1F_1(X, u) - A_2F_2(X, u) - \dot{\phi}) = -\beta z \tag{38}$$

where β is a positive constant parameter. Thus, $\dot{W}$ is negative semi-definite ($\dot{W} < 0$), and W converges to zero. Consequently,

$$\begin{aligned}S &\to 0 \quad \Rightarrow \quad x_1 \to x_{1,d} \\ z &\to 0 \quad \Rightarrow \quad x_3, x_4 \to \text{bounded}\end{aligned} \tag{39}$$

In other words, by converging S to zero, it can be concluded that x_1 converges to its desired value. On the other hand, when z converges to zero, internal states of the system, x_3 and x_4 will be bounded. By solving Eq. (38), the desired control strategy will be obtained. In [37], a similar experimental study on a haptic device, a method has been proposed for computing numerical differentiation of angles of the robot's links. This approach has been implemented in this paper for online calculation of differential terms in $\dot{\phi}$ which includes $\dot{x}_1$, $\ddot{e}_x$, and $\ddot{x}_{1,d}$. The following equations describe the numerical differentiation approach as follows:

$$\dot{x} = \sum_{i=1}^{N}\sum_{j=i+1}^{N}\frac{w\left(\frac{t_i+t_j}{2} - c\right)(x_j - x_i)}{t_j - t_i} \tag{40}$$

where x is the parameter on which the differentiation is employed, c is a constant, N stands for the length of moving window and $w(x)$ indicates Gaussian distribution function with standard deviation of σ which are formulated as:

$$w(x) = \frac{1}{\sqrt{2\pi\sigma^2}}\exp\left(\frac{-x^2}{2\sigma^2}\right) \tag{41}$$

The value of standard deviation should be determined by taking into account of two factors: (1) length of the window and (2) noise of measurement. As the window length increases the output results become more smoother whereas it may increase the error of differentiation. On the other hand, the more value the standard deviation has, the more smoother results is obtained. Thus, the standard deviation and window length should be determined for each case considering the noise level. In our experimental study, the window length and standard deviation has been set 15 and 0.85, respectively, after some trial and error.

According to [38], the relationship between input voltage, u, and spool displacement, X_{spool} of the 5/3 way MPYE-5-1/8-HF-010B Festo proportional control valve can be expressed by a linear relation as follows:

$$X_{\text{spool}} = au + b \tag{42}$$

where $a = -0.3 \times 10^{-3}$ and $b = 1.5 \times 10^{-3}$. By considering Eqs. (6) and (42), it can be concluded the mass flow rate is related to the input signal, u, by a second order polynomial function:

$$\dot{m}_{i,j}(P_u, P_d) = H_j(P_u, P_d)\frac{\pi}{4}(a\cdot u + b)^2, \quad j = 1, 2 \tag{43}$$

where $H_j(P_u, P_d)$ indicates multiplication of all variables which are coefficients of A_v in the mass flow rate equation, Eq. (4). Regarding the small values for γ_k in Table 8, the term corresponding to the output mass flow rate, $\gamma_o\dot{m}_{o,j}$ ($j = 1, 2$), can be ignored due to its small value in the dynamic equations of the PneuSys, Eq. (8). Finally, substituting the variables H, X_{spool}, and $\dot{m}_{i,j}$ into Backstepping-Sliding Mode controller strategy in Eq. (38) and some simplifications leads to the control strategies for all the six PneuSys, which aims at trajectory tracking of the robot, as follows:

$$A_1\left(\frac{RT}{V_1}\gamma_i H_1\frac{\pi}{4}(a\cdot u+b)^2-\gamma_k\left(\frac{x_3}{V_1}\right)\dot{V}_1\right)-A_2\left(\frac{RT}{V_2}\gamma_i H_2\frac{\pi}{4}(a\cdot u+b)^2 + \gamma_k\left(\frac{x_4}{V_2}\right)\dot{V}_2\right)-\beta z-\dot{\phi}=0$$

$$u=\frac{1}{a}\left(\frac{A_1\gamma_k x_3\dot{V}_1/V_1-A_2\gamma_k x_4\dot{V}_2/V_2+\beta z+\dot{\phi}}{\frac{\pi}{4}(A_1RT\gamma_i H_1/V_1-A_2RT\gamma_o H_2/V_2)}\right)^{1/2}-\frac{b}{a} \quad (44)$$

where u is the control signal. It should be noted that the denominator of the control signal will never be equal to zero because $A_1\gamma_i H_1 V_2 \neq A_2\gamma_o V_1 H_2$ for all the values of upstream and downstream pressures.

The ϕ includes the switching term, $K\text{sgn}(s)$, in the sliding mode controller. The use of sgn(s) in the controller design will cause serious problems in practical tests. Thus, the tanh (.) function has been employed in the practical tests of the robot. Thus, referring to Eq. (38), the ϕ can be approximated to:

$$\phi \simeq \hat{\phi} - K\tanh(\xi s) \quad (45)$$

where ξ is a constant value which has been set 10. The tanh (.) function provides a smooth transitions close to zero where the sliding mode controller is switched. The approximated ϕ is computed online and its first derivative, $\dot{\phi}$, is obtained by employing the aforementioned proposed method of differentiation in Eq. (40). As a result, by using the tanh (.) function instead of sgn(s), the ϕ would be differentiable and also computable.

4. Trajectory tracking control of the hexataar robot based on Back-Stepping Sliding Mode controller and geometry-based quasi-forward kinematic method

In this section, the control strategy is described which employs the task space and joint space control, simultaneously. The proposed closed-loop control method is based on employing BS-SMC and using GQFK method. Furthermore, trajectory tracking control of the HexaTaar robot is performed for different trajectories including pure sinusoidal motions and more complicated sinusoidal motion. Besides, data obtained from experimental results are reported in tables and figures.

4.1. The closed-loop proposed control strategy

The joint space control is performed according to the calculated error between the desired lengths of the actuators and the measured lengths via potentiometer. On the other hand, the task space control is based on comparing desired trajectory and the calculated pose (position and orientation) of the E-E. Fig. 7 demonstrates schematic of the proposed control strategies for the control of the HexaTaar robot.

In [39], the kinematic equations of the same Gough–Stewart robot, HexaTaar, has been derived and the novel method for calculating position of the end-effector, GQFK, has been explained. Referring to [39], the kinematic equations of the HexaTaar robot can be written as follows:

$$l_i=[{}^A\mathbf{p}^T{}^A\mathbf{p}+{}^A\mathbf{b}_i^T{}^A\mathbf{b}_i+{}^A\mathbf{a}_i^T{}^A\mathbf{a}_i-2{}^A\mathbf{p}^T{}^A\mathbf{a}_i+2{}^A\mathbf{p}^T[{}^A\mathbf{R}_B{}^B\mathbf{b}_i]-2[{}^A\mathbf{R}_B{}^B\mathbf{b}_i]^T\mathbf{a}_i]^{1/2} \quad (46)$$

where l_i, $\mathbf{p}$, $\mathbf{s}_i$, and $\mathbf{R}_B$ stand for length of the links, position of the end-effector, and rotation matrix, respectively. Moreover, location of the joints are indicated by $\mathbf{a}_i$, $\mathbf{b}_i$ in their local frame. Furthermore, the closed-form formulation of the GQFK method has been explained in [39] which is written as follows:

$$\mathbf{P}=\mathbf{O}_1+\frac{1}{2}\left(1+\frac{r_1^2-r_3^2}{\|\mathbf{O}_3-\mathbf{O}_1\|^2}\right)(\mathbf{O}_3-\mathbf{O}_1)+\frac{1}{2\|\hat{\mathbf{d}}\|}\left(\left\|\mathbf{O}_5-\mathbf{O}_1\right\|^2+r_1^2-r_5^2-\left(1+\frac{r_1^2-r_3^2}{\|\mathbf{O}_3-\mathbf{O}_1\|^2}\right)(\mathbf{O}_3-\mathbf{O}_1)(\mathbf{O}_5-\mathbf{O}_1)\right)\times(\hat{\mathbf{d}}\times(\mathbf{O}_3-\mathbf{O}_1))$$
$$\pm\left(\left(r_1^2-\left\{-\frac{1}{4}\left(1+\frac{r_1^2-r_5^2}{\|\mathbf{O}_3-\mathbf{O}_1\|}\right)^2+\frac{1}{4\|\hat{\mathbf{d}}\|^2}\left(\left\|\mathbf{O}_5-\mathbf{O}_1+r_1^2-r_5^2-\left(1+\frac{r_1^2-r_3^2}{\|\mathbf{O}_3-\mathbf{O}_1\|^2}\right)(\mathbf{O}_3-\mathbf{O}_1)(\mathbf{O}_5-\mathbf{O}_1)\right\|^2\right)^2\right\}\|\mathbf{O}_3-\mathbf{O}_1\|^2\right)^{1/2}\right)\hat{\mathbf{d}} \quad (47)$$

where the length of l_is represent the radius of six spheres with the origin of $\mathbf{O}_i$ vectors which are $\mathbf{O}_i=\mathbf{a}_i-\mathbf{R}\mathbf{b}_i$. The $\hat{\mathbf{d}}$ and $\hat{\mathbf{d}}$ indicate the normal and unit vectors of the plane including the origins of the corresponding spheres, respectively.

According to Fig. 7, the desired lengths of the six links are calculated directly, by solving inverse kinematic equations, for the desired pose of the E-E. The lengths of the links in practice, which are measured by the potentiometers, are compared to the desired lengths. Then, the Backstepping-Sliding Mode controller is employed end of to the eliminating the error of the links' lengths in the joint space.

In the task space control (outer loop), pose of the E-E including rotation of the E-E which is measured by IMU sensor and its position which is computed by the GQFK method is compared with the predefined desired trajectory to obtain the pose error. The task space error can be mapped into the joint space error using the Jacobian matrix of the HexaTaar robot. Regarding to [40], the Jacobian matrix of the 6-

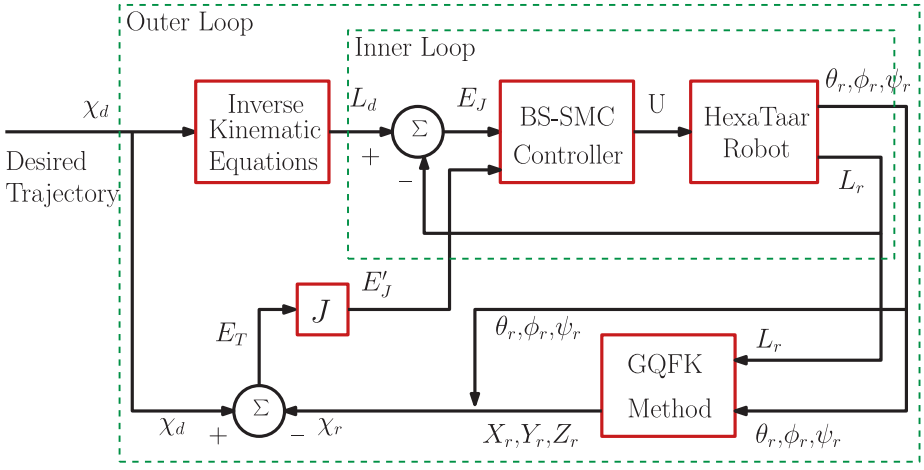

Fig. 7. Schematic of the closed-loop control of the 6-DoF HexaTaar robot.

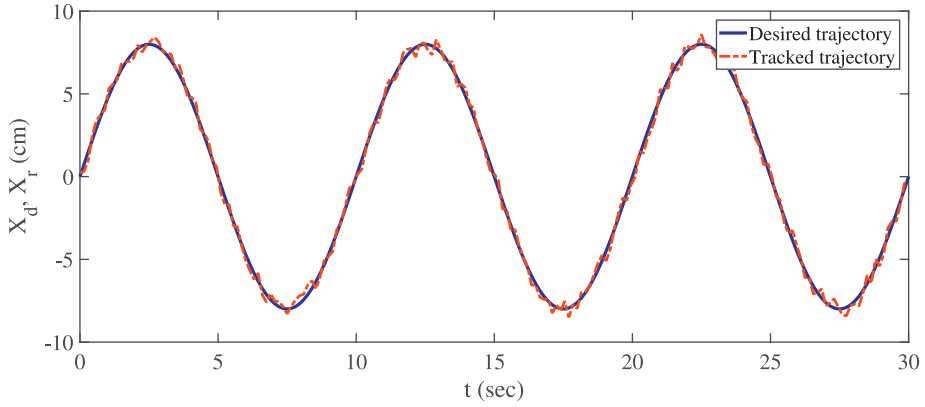

Fig. 8. The desired and tracked pure translation along the *X* axis.

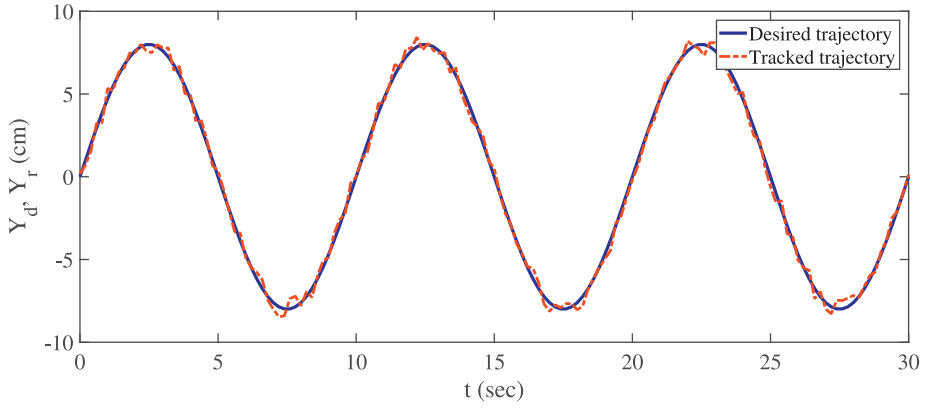

Fig. 9. The desired and tracked pure translation along the *Y* axis.

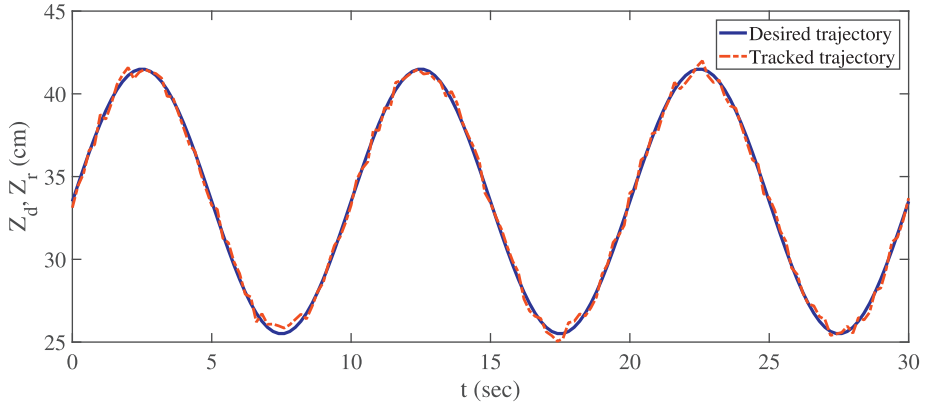

Fig. 10. The desired and tracked pure translation along the *Z* axis.

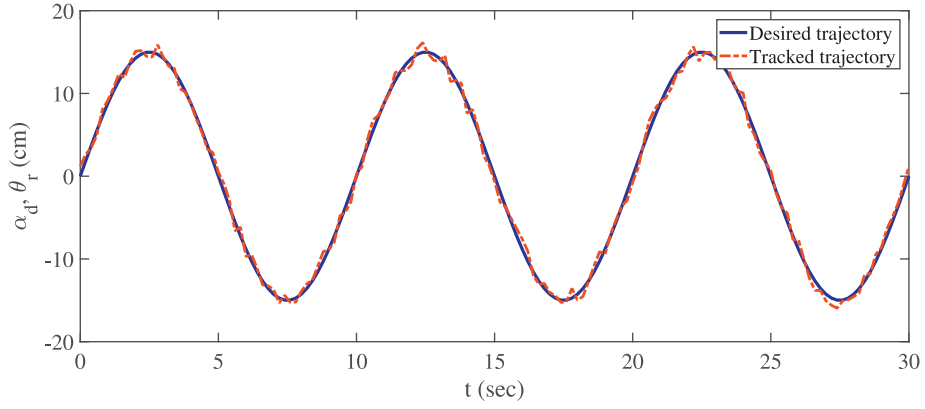

Fig. 11. The desired and tracked pure rotation around the *X* axis.

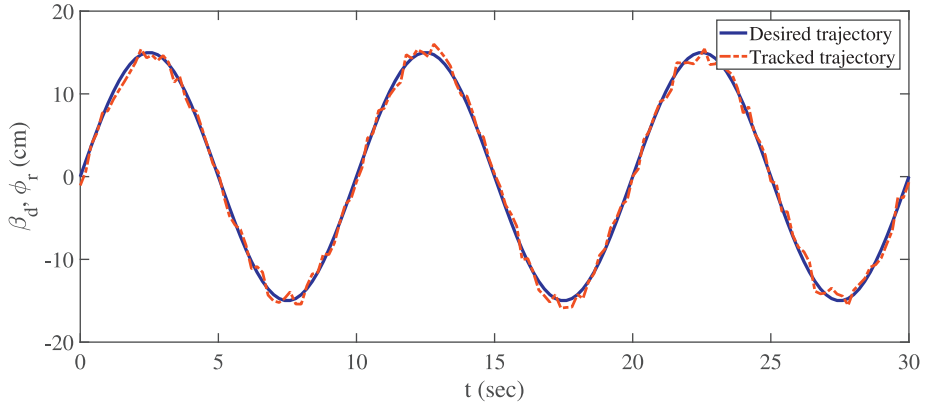

Fig. 12. The desired and tracked pure rotation around the *Y* axis.

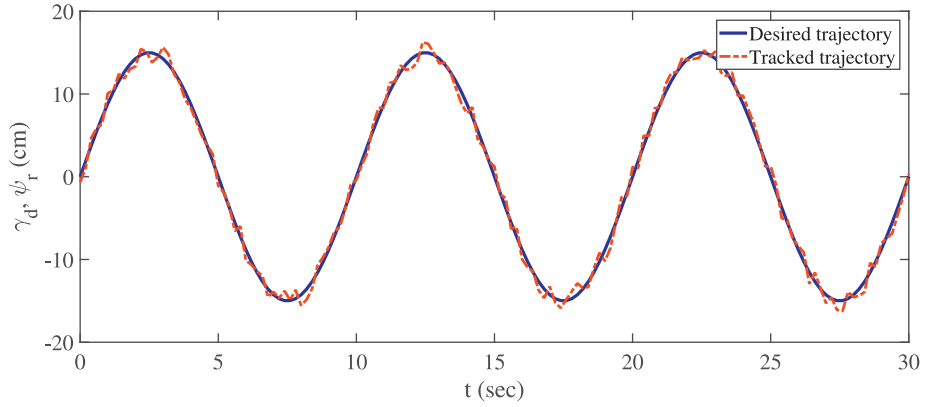

Fig. 13. The desired and tracked pure rotation around the *Z* axis.

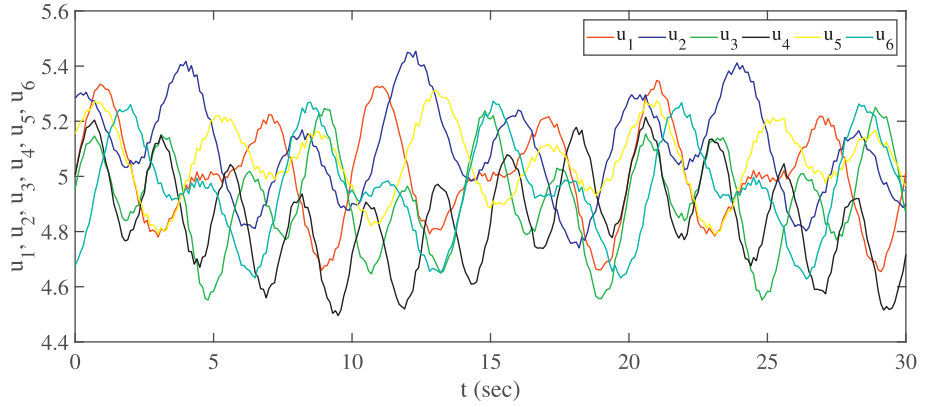

Fig. 14. The control signals for each link of the robot in tracking of pure translation along the *X* axis.

DoF HexaTaar robot which is a 6 × 6 square matrix can be determined expressed by using the screw theory notation as follows: Geometry-based Quasi Forward Kinematic (GQFK) method

$$\mathbf{J} = \begin{bmatrix} \mathbf{s}_1 & \mathbf{s}_2 & \mathbf{s}_3 & \mathbf{s}_4 & \mathbf{s}_5 & \mathbf{s}_6 \\ (\mathbf{b}_1 \times \mathbf{s}_1) & (\mathbf{b}_2 \times \mathbf{s}_2) & (\mathbf{b}_3 \times \mathbf{s}_3) & (\mathbf{b}_4 \times \mathbf{s}_4) & (\mathbf{b}_5 \times \mathbf{s}_5) & (\mathbf{b}_6 \times \mathbf{s}_6) \end{bmatrix}^T \tag{48}$$

where s_i indicates direction of ith link and $\mathbf{b}_i$ represents the moving attachment points of the links to the End-Effector. Thus, the error of the links' lengths corresponding to the pose error will be obtained. Consequently, the control signals are generated based on two sets of error: (1) The difference between desired lengths of the links and the measured length by the potentiometers, (2) The length of the links' error which is transformed from task space into joint space by the Jacobian matrix.

In the proposed control method, the errors from the outer control loop is transformed to the inner control loop via Jacobian matrix in Eq. (48), after each 5 cycles of the inner control loop. The mapped error (from the task space to the joint space) contains valuable information of the errors in tracking of the E-E's position and rotation. These errors are employed to tune the errors of the links' length in order to eliminate errors which are generated from : (1) Inaccuracy in measuring the lengths and angles of the mechanical parts of the HexaTaar robot, which leads to errors in kinematic equations and (2) Errors in data obtained from the potentiometer and IMU sensors.

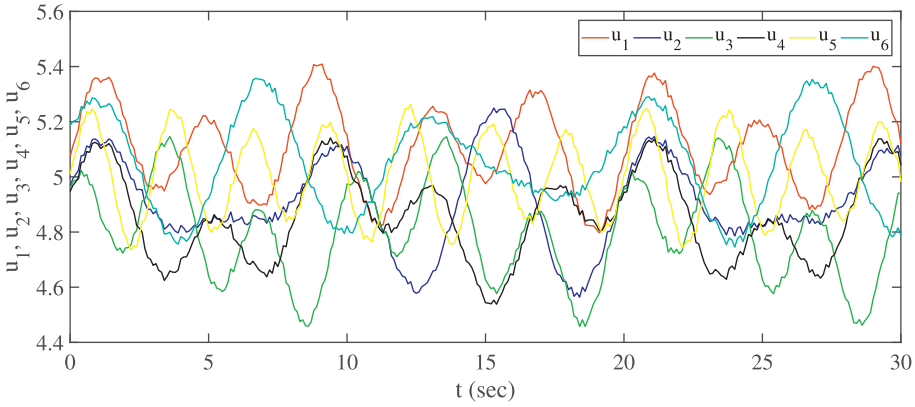

Fig. 15. The control signals for each link of the robot in tracking of pure translation along the *Y* axis.

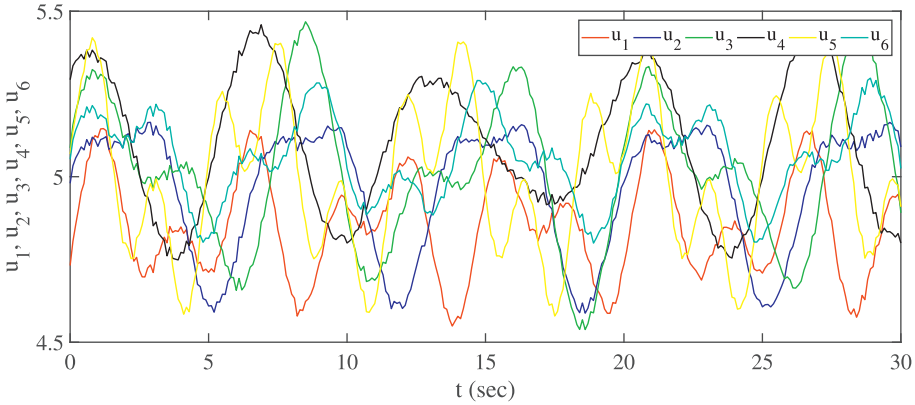

Fig. 16. The control signals for each link of the robot in tracking of pure translation along the *Z* axis.

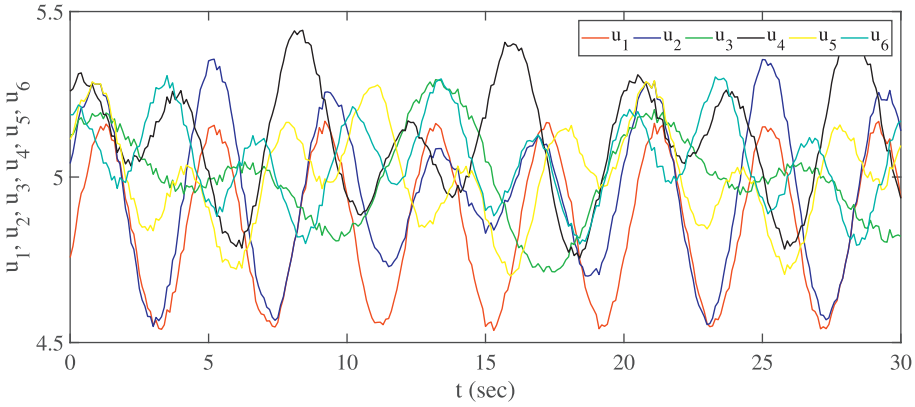

Fig. 17. The control signals for each link of the robot in tracking of pure rotation around the *X* axis.

The both sets of errors in Fig. 7, E_J and $\acute{E}_J$, are utilized in the proposed control strategy. The inner and outer control loops have different speeds. It is worthwhile to know that it takes approximately 5 to 6 (ms) a cycle of main loop of the written program in Arduino. Since the inner loop is 5 times faster than the outer loop, the error signals from task and joint spaces should be used in a proper way. In the experimental tests, it take approximately 1 (ms) and 5 (ms) respectively for the inner outer loop to give feedback of the errors. Thus, one can consider a cycle of 5 (sec) for performance of the controller, which has 5 main steps of 1 (ms). The E_J is considered for the first four steps and the $\acute{E}_J$ is employed in the last step. In other words, the feedback of errors in the joint space of the robot guarantee that the actuators would track the desired trajectory. By this way, the errors are compensated at each step of 1 (ms), which eventually prevents accumulation of errors. Assuming the E_J is ignored, if the controller only employs the $\acute{E}_J$ at the end of each 5 (ms) cycle, the desired trajectory are tracked but with large values of error. Although the measured error in the task space primarily indicate performance of the proposed control strategy, the joint space feedback is required to improve its performance in trajectory tracking control of the robot.

4.2. Tracking sinusoidal motions through each DoF

Desired translations along and rotations around the three axes, *X, Y* and *Z* are considered for trajectory tracking. Thus, six different sinusoidal trajectories are experimented with frequency of 0.1(Hz) and

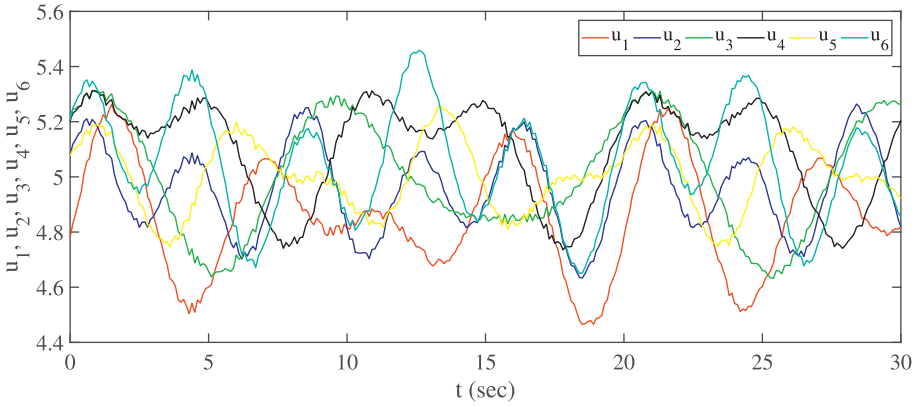

Fig. 18. The control signals for each link of the robot in tracking of pure rotation around the *Y* axis.

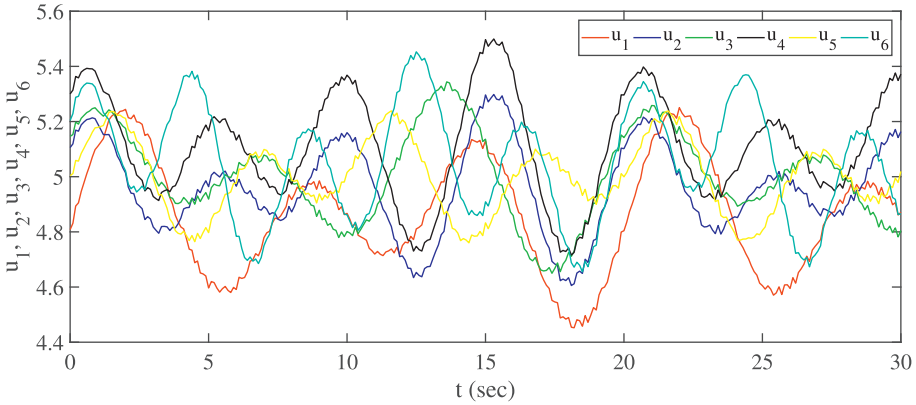

Fig. 19. The control signals for each link of the robot in tracking of pure rotation around the *Z* axis.

Table 9
Root Mean Square Error (RMSE) of trajectory tracking for pure translations and rotations.

	Translation (cm)			Rotation (deg)		
	X	*Y*	*Z*	*X*	*Y*	*Z*
RMSE	0.782	0.841	0.197	1.012	1.346	1.836
Relative error	4.86%	6.53%	2.31%	7.47%	8.12%	9.33%

amplitude of 8(cm) and 15(deg) for pure translations and rotations. Moreover, IMU sensor measures rotations in practice and the positions are computed based on the GQFK method during tracking the desired trajectories.

Figs. 8–10 demonstrate the desired and tracked trajectories for all the pure translational trajectories of the E-E. Moreover, the desired and tracked trajectories for all the pure rotation trajectories of the E-E have been shown in Figs. 11–13. The parameters X_d, Y_d and Z_d indicate the desired translations and the parameters α_d, β_d and γ_d represent the desired rotations. The parameters X_r, Y_r, Z_r, θ_r, ϕ_r and ψ_r indicate the

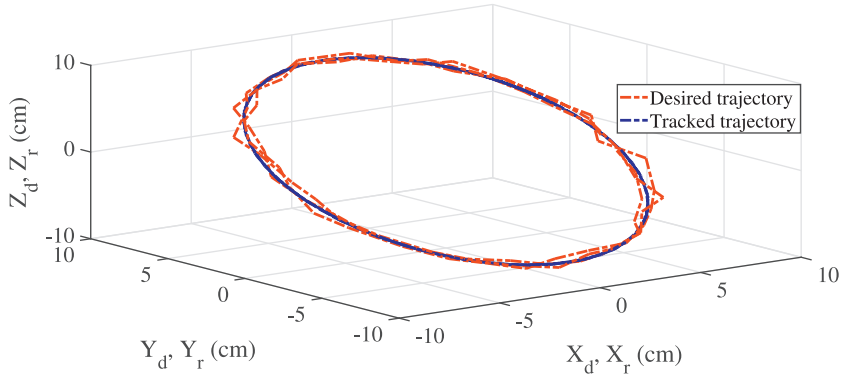

Fig. 20. 3-D overview of tracking complicated sinusoidal trajectory.

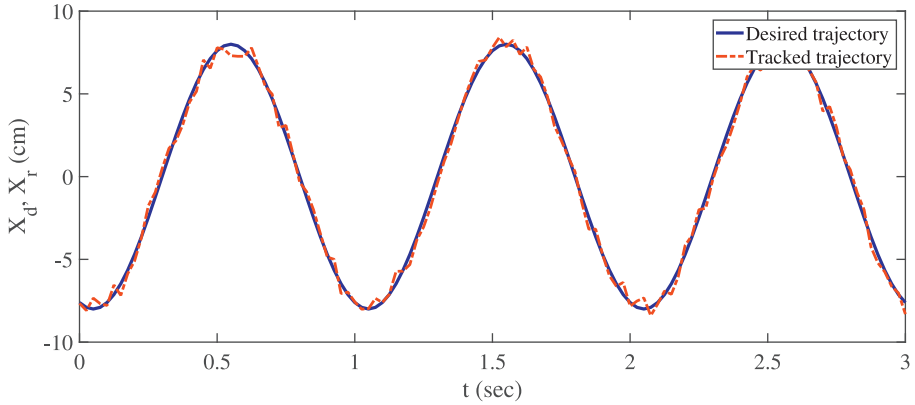

Fig. 21. The desired and tracked translation along the *X* axis for the complicated sinusoidal trajectory.

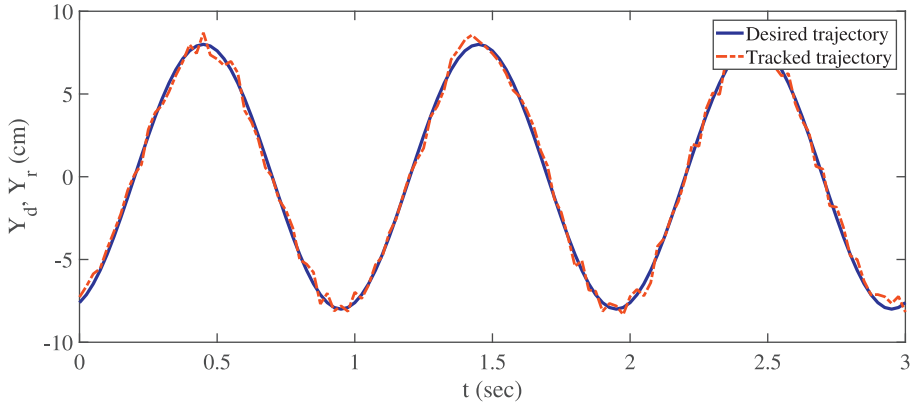

Fig. 22. The desired and tracked translation along the *Y* axis for the complicated sinusoidal trajectory.

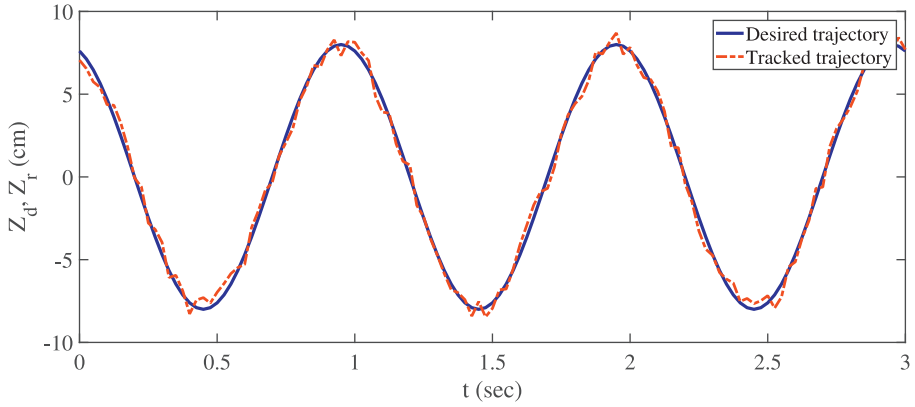

Fig. 23. The desired and tracked translation along the *Z* axis for the complicated sinusoidal trajectory.

measured pose of the E-E. Figs. 14–19 demonstrate the control signals for each link of the robot during tracking of the pure sinusoidal motions. The Root Mean Square Error (RMSE) of trajectory tracking is reported in Table 9. According to the measured errors, pure motions are tracked properly, approximately, lower than 2 (cm) in translations and 4 (deg) in rotations, by employing the proposed controller.

4.3. Tracking complicated trajectories

Trajectories in most applications of the 6-DoF platform is a combination of rotation and translation. Consider a desired three dimensional sinusoidal trajectory in which translations and rotations are indicated by $\chi_d = [X_d, Y_d, Z_d, \alpha_d, \beta_d, \gamma_d]$ are as follows:

$$\text{Desired translation:} \begin{cases} X_d = 8\sin(2\pi \times 1 \times t) \\ Y_d = 8\cos(2\pi \times 1 \times t) \\ Z_d = 8\sin(2\pi \times 1 \times t) \end{cases}$$
$$\text{Desired rotation:} \begin{cases} \alpha_d = 0 \\ \beta_d = 0 \\ \gamma_d = 0 \end{cases} \quad (49)$$

Figs. 21–23 exhibit tracking the desired trajectories along the *X, Y* and *Z* axes. Furthermore, Fig. 20 shows the 3-D overview of the 6-DoF HexaTaar parallel robot during tracking of the more complicated desired sinusoidal trajectory. Moreover, Figs. 24–29 demonstrate tracking of the desired lengths of the links in which the cylinders' displacement are

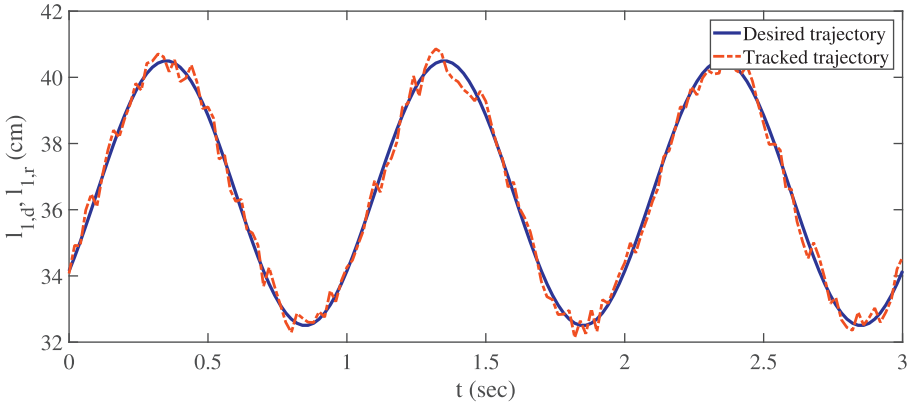

Fig. 24. The desired and tracked length of link 1 for the complicated sinusoidal desired trajectory.

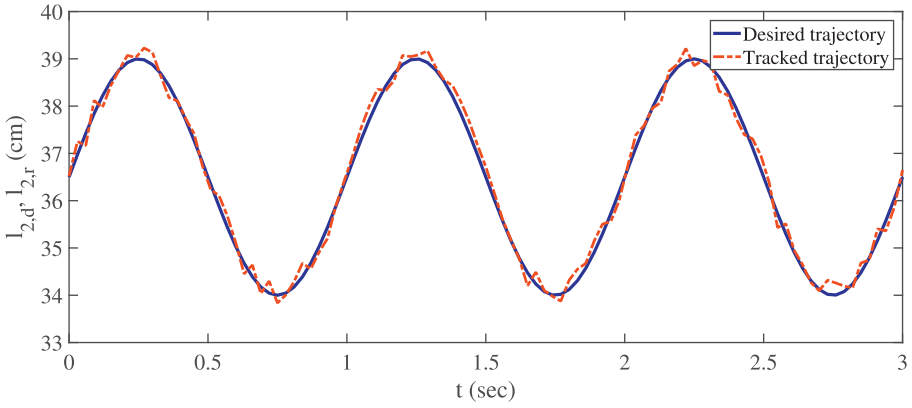

Fig. 25. The desired and tracked length of link 2 for the complicated sinusoidal trajectory.

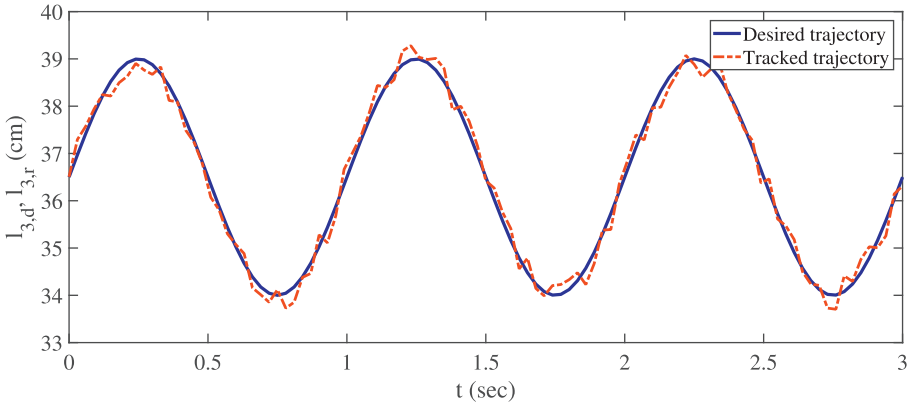

Fig. 26. The desired and tracked length of link 3 for the complicated sinusoidal trajectory.

measured by the corresponding potentiometer. Moreover, the Figs. 30 depicts the control signals for each link of the robot in tracking of the complicated trajectory. The RMSE criterion for translations and rotations of the aforementioned combinational trajectory are listed in Table 10.

Referring to [11], which was a previous study carried out on the control of the HexaTaar robot, a conventional control algorithm, PI, have been employed in order to control the Gough–Stewart robot. Although the errors for position of the links were reported 0.0254 (cm) in steady state after 4(s) and more, the errors of the position were reported approximately 1.106(cm) for times smaller than 1(s). In turn, the errors for positions of the links must take small values in the beginning seconds of the actuators' motion in order to have a suitable performance in trajectory tracking control of the robot. The results reported in [11], reveals that the amounts of error for the position of the links, will lead to large errors in the task space control. Consequently, such

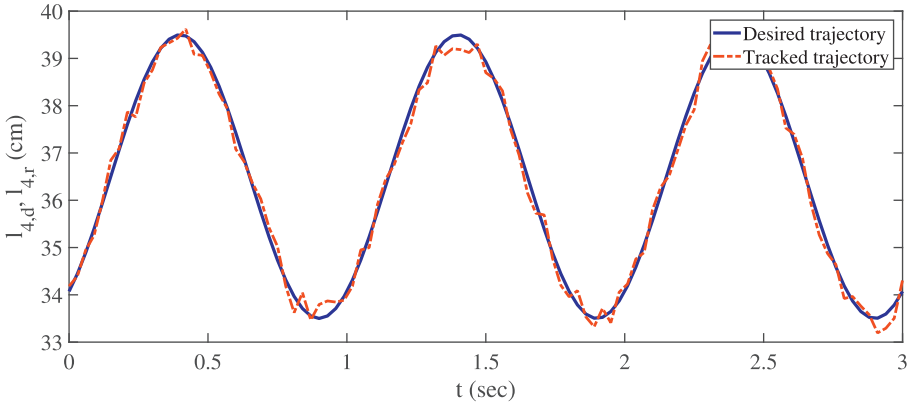

Fig. 27. The desired and tracked length of link 4 for the complicated sinusoidal trajectory.

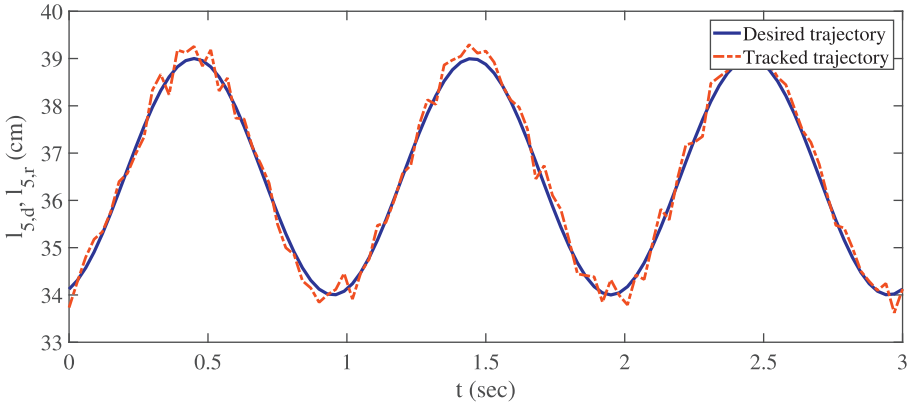

Fig. 28. The desired and tracked length of link 5 for the complicated sinusoidal trajectory.

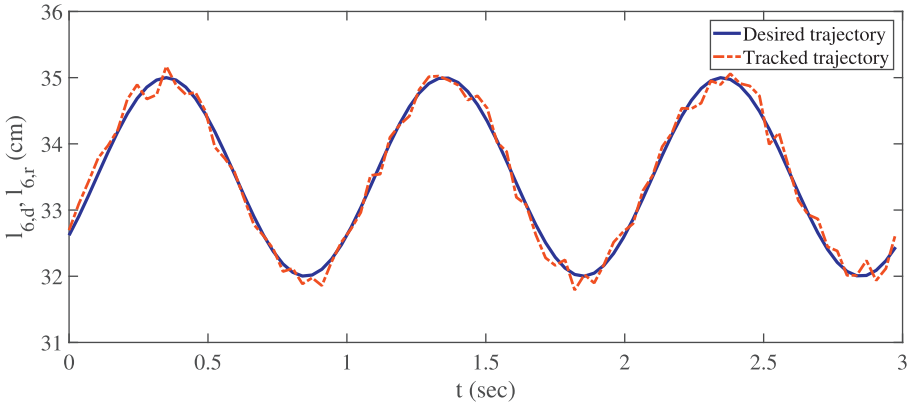

Fig. 29. The desired and tracked length of link 6 for the complicated sinusoidal trajectory.

conventional controllers, e.g. PI and PID, would not contribute to appropriate results in trajectory tracking control of the robot and justify the use of Backstepping-Sliding Mode control strategy for this purpose.

5. Conclusion

This paper addressed the trajectory tracking control of a 6-DOF pneumatically actuated Gough-Stewart parallel robot, namely HexaTaar. To this end, dynamic model of the pneumatic system of each link of the HexaTaar robot were extracted including dynamic equations of the pneumatic cylinders and the proportional electrical valves. The obtained dynamic model includes unknown parameters which were identified using Genetic Algorithm. Moreover, position control of the pneumatic actuator was performed by designing a nonlinear controller, the so-called Back-Stepping Sliding Mode. Kinematic equations of the 6-DOF robot were derived and a novel method, the so-called Geometry Quasi-Forward Kinematic method, was proposed for calculating position of the End-Effector based on the intersection of spheres and data

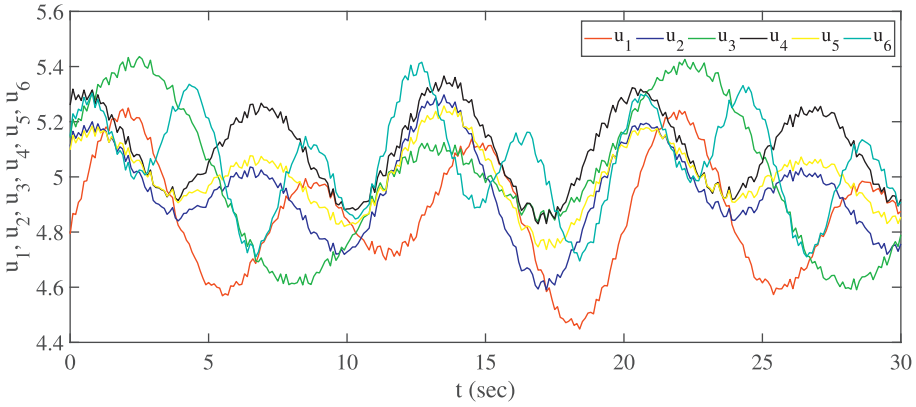

Fig. 30. 3-D overview of tracking complicated sinusoidal trajectory.

Table 10
Root Mean Square Error (RMSE) of trajectory tracking for the complicated sinusoidal trajectory.

	Translation (cm)			Rotation (deg)		
	X	*Y*	*Z*	*X*	*Y*	*Z*
RMSE	0.845	1.205	0.296	1.193	1.817	2.433
Relative Error	5.19%	6.33%	3.89%	5.51%	7.65%	8.32%

gathered by rotation sensors. A closed-loop control was designed based on two control loops including joint space and task space control, simultaneously. Furthermore, trajectory tracking control of the robot was performed for different desired trajectories which resulted in an appropriate performance in tracking approximately lower than 2 (cm) and 4 (deg) in translations and rotations, respectively. From the experimental results, it can be inferred that the proposed Back-Stepping Sliding Mode controller and the Geometry-based Quasi-Forward Kinematic method can be employed for trajectory tacking control of the 6-DoF HexaTaar parallel robot. As ongoing works, the proposed methods can be extended for controlling different parallel robots, e.g., Delta and cable-driven robots, in various applications such as leg or hand rehabilitation, earthquake and flight simulators.

Appendix A

In this Appendix, the dynamic equations of the PneuSys includes the dynamics of the piston and the proportional valve are obtained according to Eqs. (50) to (63) formulated by Richer et. al in [34]. The piston dynamics is as follows:

$$(M_L + M_p)\ddot{x} + \beta\dot{x} + F_f + F_L = P_1A_1 - P_2A_2 - P_aA_r \tag{50}$$

where M_L is the mass of the load, M_p is the mass of the piston, x is the position of the piston, β is the viscous coefficient, F_f is the Coulomb friction force, F_L is the gravity force, P_1 and P_2 are the air pressures in chambers of the actuator which are measured by pressure sensors, P_a is the atmosphere pressure, A_1 and A_2 are the piston areas at its both ends, and A_r is the rod area of the piston.

The dynamic equations of the pressure through the proportional valve is obtained as follows:

$$P = \rho RT \tag{51}$$

where, R is the constant parameter of ideal gas. Applying the continuity equation the mass flow rate can be expressed as,

$$\dot{m} = \frac{d}{dt}(\rho V) \tag{52}$$

which can be obtained as,

$$\dot{m}_{\text{in}} - \dot{m}_{\text{out}} = \dot{\rho}V + \rho\dot{V} \tag{53}$$

where, $\dot{m}_{\text{in}}$ and $\dot{m}_{\text{out}}$ are inlet and outlet mass flow rates of the chambers. The energy equation can be written as follows:

$$q_{\text{in}} - q_{\text{out}} + kC_v(\dot{m}_{\text{in}}T_{\text{in}} - \dot{m}_{\text{out}}T_{\text{out}}) - \dot{W} = \dot{U} \tag{54}$$

where q_{in} and q_{out} indicate heat transfer, k is the specific heat ratio, C_v is the specific heat at constant volume, T_{in} is the temperature of the input air flow, $\dot{W}$ is the rate of change in the work, and $\dot{U}$ is the change of internal energy [34]. The variation of internal energy is,

$$\dot{U} = \frac{d}{dt}(C_vmT) = \frac{1}{k-1}\frac{d}{dt}(PV) = \frac{1}{k-1}(V\dot{P} + P\dot{V}) \tag{55}$$

in which the ideal gas formula of specific heat ratio, $C_v = R/(k1)$, is considered. By substituting $\dot{W} = P\dot{V}$ and Eq. (55) into Eq. (54), on has:

$$q_{\text{in}} - q_{\text{out}} + \frac{k}{k-1}\frac{P}{\rho T}(\dot{m}_{\text{in}}T_{\text{in}} - \dot{m}_{\text{out}}T) - \frac{k}{k-1}P\dot{V} = \frac{1}{k-1}V\dot{P} \tag{56}$$

Thus, the energy equation becomes:

$$\frac{k}{k-1}(\dot{q}_{\text{in}} - \dot{q}_{\text{out}}) + \frac{1}{\rho}(\dot{m}_{\text{in}} - \dot{m}_{\text{out}}) - \dot{V} = \frac{V}{kP}\dot{P} \tag{57}$$

If the process is considered to be adiabatic ($q_{\text{in}} - q_{\text{out}} = 0$), the time derivative of the chamber pressure is,

$$\dot{P} = k\frac{P}{\rho V}(\dot{m}_{\text{in}} - \dot{m}_{\text{out}}) - k\frac{P}{V}\dot{V} \tag{58}$$

or, substituting ρ from Eq. (51),

$$\dot{P} = k\frac{RT}{V}(\dot{m}_{\text{in}} - \dot{m}_{\text{out}}) - k\frac{P}{V}\dot{V} \tag{59}$$

If the process is considered to be isothermal (T = constant), then the change in internal energy is,

$$\dot{U} = C_v \dot{m} T \tag{60}$$

and Eq. (57) can be written as:

$$q_{\text{in}} - q_{\text{out}} = P\dot{V} - \frac{P}{\rho}(\dot{m}_{\text{in}} - \dot{m}_{\text{out}}) \tag{61}$$

Then, the rate of change in pressure will be,

$$\dot{P} = \frac{RT}{V}(\dot{m}_{\text{in}} - \dot{m}_{\text{out}}) - \frac{P}{V}\dot{V} \tag{62}$$

A comparison of Eqs. (59) and (62) shows that the only difference is the specific heat ratio term k. Thus, both equations can be written as,

$$\dot{P} = \frac{RT}{V}(\alpha_{\text{in}}) \tag{63}$$

where α, α_{in}, and α_{out} take values between 1 and k, depending on the actual heat transfer during the process [34]. Thus, the exact value of heat transfer variables cannot be measured. The coefficients α, α_{in}, and α_{out} should be estimated, which can be identified by experimental tests.

The reference position of the piston is in the middle of the stroke. The volume of each chamber can be expressed as,

$$V_i = V_{0i} + A_i\left(\frac{1}{2}L \pm x\right) \tag{64}$$

where $i = 1, 2$ indicates chambers' index, V_{0i} is the inactive volume at the end of stroke and admission ports, A_i is the piston effective area, L is the piston stroke, and x is the piston position. The difference between the piston effective areas for each chamber A_1 and A_2 is due to the piston rod [34]. Finally, by substituting Eq. (64) into Eq. (63), the last two equations of dynamic of pressures in chambers are obtained as follows:

$$\dot{P}_i = \frac{RT}{V_{0i} + A_i(0.5L \pm x)}(\alpha_{in}\dot{m}_{in} - \alpha_{out}\dot{m}_{out}) - \alpha\frac{PA_i}{V_{0i} + A_i(0.5L \pm x)} \tag{65}$$

Appendix B

In this Appendix, the details of obtaining the Coulomb friction and the viscous coefficient are described.

In [36], calculation of Coulomb friction and viscous coefficient using the Free-Fall test has been explained in details. Regarding the following equation, the differential equation of motion for the piston is:

$$\ddot{x} = g - \frac{g}{W}F_{fric} - \frac{g}{W}b\dot{x} \tag{66}$$

where the initial conditions of Eq. 66 are $x = 0$ and $\dot{x} = 0$. The general solution to the differential equation is:

$$x = A(t + \tau\exp(-t/\tau) - \tau) \tag{67}$$

where A is a constant and τ is the time constant of the solution. According to Eqs. (66) and (67) one has:

$$\frac{A}{\tau}\exp(-t/\tau) = g - \frac{g}{W}F_{fric} - \frac{g}{W}bA\left(1 - \exp\left(\frac{-t}{\tau}\right)\right) \tag{68}$$

and after rearranging becomes:

$$A\exp\left(\frac{-t}{\tau}\right)\left(\frac{1}{\tau} - \frac{g}{W}b\right) = g - \frac{g}{W}F_{fric} - \frac{g}{W}bA \tag{69}$$

By applying the boundary conditions to Eq. (69), the unknown parameters of Coulomb friction and viscous coefficient can be calculated. For $t = 0$:

$$A\left(\frac{1}{\tau} - \frac{g}{W}b\right) = g - \frac{g}{W}F_{fric} - \frac{g}{W}bA \tag{70}$$

and for $t = \infty$,

$$0 = g - \frac{g}{W}F_{fric} - \frac{g}{W}bA \tag{71}$$

Thus, F_{fric} and b can be expressed in terms of A and τ as follows:

$$\begin{aligned} F_{fric} &= W\left(1 - \frac{A}{g\tau}\right) \\ b &= \frac{W - F_{fric}}{A} \end{aligned} \tag{72}$$

References

[1] J.-P. Merlet, Parallel Robots, 74 Springer Science & Business Media, 2012.
[2] H. Tari, H.-J. Su, J.D. Hauenstein, Classification and complete solution of the kinetostatics of a compliant Stewart–Gough platform, Mech. Mach. Theory 49 (2012) 177–186.
[3] A. Cirillo, P. Cirillo, G.D. Maria, A. Marino, C. Natale, S. Pirozzi, Optimal custom design of both symmetric and unsymmetrical hexapod robots for aeronautics applications, Robot Comput. Integr. Manuf. 44 (2017) 1–16.
[4] L. Yingjie, Z. Wenbai, R. Gexue, Feedback control of a cable-driven Gough-Stewart platform, IEEE Trans. Rob. 22 (1) (2006) 198–202.
[5] J. Cabrera, A. Ortíz, A. Simón, F. García, A.P.L. Blanca, A versatile flat track tire testing machine, Veh. Syst. Dyn. 40 (4) (2003) 271–284.
[6] X. Duan, Y. Qiu, J. Mi, H. Bao, On the mechatronic servo bandwidth of a Stewart platform for active vibration isolating in a super antenna, Robot Comput. Integr. Manuf. 40 (2016) 66–77.
[7] A. Valera, M. Díaz-Rodríguez, M. Valles, E. Oliver, V. Mata, A. Page, Controller observer design and dynamic parameter identification for model-based control of an electromechanical lower-limb rehabilitation system, Int. J. Control 90 (4) (2017) 702–714.
[8] A. Rastegarpanah, M. Saadat, A. Borboni, Parallel robot for lower limb rehabilitation exercises, Appl. Bionics Biomech. 2016 (2016).
[9] Y. Pi, X. Wang, Trajectory tracking control of a 6-dof hydraulic parallel robot manipulator with uncertain load disturbances, Control Eng. Pract. 19 (2) (2011) 185–193.
[10] G. Asaeikheybari, A. Salimi Lafmejani, A. Kalhor, M.T. Masouleh, Dimensional synthesis of a four-bar linkage mechanism via a pso-based cooperative neural network approach, Proceedings of the Iranian Conference on Electrical Engineering (ICEE), IEEE, 2017, pp. 906–911.
[11] J.H. Machiani, M.T. Masouleh, A. Kalhor, M.G. Tabrizi, F. Sanie, Control of a pneumatically actuated 6-dof Gough-Stewart platform, Proceedings of the Second RSI/ISM International Conference on Robotics and Mechatronics (ICRoM), (2014), pp. 166–171.
[12] J. Cazalilla, M. Vallés, Ángel Valera, V. Mata, M. Díaz-Rodríguez, Hybrid force/position control for a 3-dof 1t2r parallel robot: implementation, simulations and experiments, Mech. Based Des. Struct. Mach. 44 (1,2) (2016) 16–31.
[13] S.-K. Song, D.-S. Kwon, Efficient formulation approach for the forward kinematics of 3–6 parallel mechanisms, Adv. Rob. 16 (2) (2002) 191–215.
[14] R. Chellal, L. Cuvillon, E. Laroche, Model identification and vision-based h position control of 6-dof cable-driven parallel robots, Int. J. Control 90 (4) (2017) 684–701.
[15] A. Salimi Lafmejani, A. Kalhor, M. Tale Masouleh, A new development of homotopy continuation method, applied in solving nonlinear kinematic system of equations of parallel mechanisms, Proceedings of the Third RSI International Conference on Robotics and Mechatronics (ICROM), (2015), pp. 737–742.
[16] A. Mahmoodi, A. Sayadi, M.B. Menhaj, Solution of forward kinematics in stewart platform using six rotary sensors on joints of three legs, Adv. Rob. 28 (1) (2014) 27–37.
[17] A. Salimi Lafmejani, M. Tale Masouleh, A. Kalhor, An experimental study on friction identification of a pneumatic actuator and dynamic modeling of a proportional valve, Proceedings of the Fourth International Conference on Robotics and Mechatronics (ICROM), (2016), pp. 166–172.
[18] K.S. Grewal, R. Dixon, J. Pearson, LQG controller design applied to a pneumatic Stewart-Gough platform, Int. J. Autom. Comput. 9 (1) (2012) 45–53.
[19] D. Pršić, N. Nedić, V. Stojanović, A nature inspired optimal control of pneumatic-driven parallel robot platform, Proc. Inst. Mech. Eng. Part C J. Mech. Eng. Sci. 231 (1) (2017) 59–71.
[20] H. Takemura, T. Onodera, D. Ming, H. Mizoguchi, Design and control of a wearable stewart platform-type ankle-foot assistive device, Int. J. Adv. Rob. Syst. 9 (5) (2012) 202.
[21] Q. Zhao, N. Wang, B.F. Spencer Jr, Adaptive position tracking control of electro-hydraulic six-degree-of-freedom driving simulator subject to perturbation, Simulation 91 (3) (2015) 265–275.
[22] B. Achili, B. Daachi, Y. Amirat, A. Ali-cherif, A robust adaptive control of a parallel robot, Int. J. Control 83 (10) (2010) 2107–2119.
[23] H. Abdellatif, B. Heimann, Advanced model-based control of a 6-dof hexapod robot: a case study, IEEE/ASME Trans. Mechatron. 15 (2) (2010) 269–279.
[24] E. Yime, R. Saltaren, J. Diaz, Robust adaptive control of the Stewart-Gough robot in the task space, Proceedings of the American Control Conference (ACC), IEEE, 2010, pp. 5248–5253.
[25] A. Salimi Lafmejani, M. Tale Masouleh, A. Kalhor, Position control of a 6-dof pneumatic Gough-Stewart parallel robot using backstepping-sliding mode controller, Mod. Mech. Eng. 17 (10) (2017) 101–111.
[26] R. Kumar, A. Chalanga, B. Bandyopadhyay, Smooth integral sliding mode controller for the position control of stewart platform, ISA Trans. 58 (2015) 543–551.
[27] N. Andreff, P. Martinet, Unifying kinematic modeling, identification, and control of a Gough–Stewart parallel robot into a vision-based framework, IEEE Trans. Rob. 22 (6) (2006) 1077–1086.
[28] S. Briot, V. Rosenzveig, P. Martinet, E. Özgür, N. Bouton, Minimal representation for the control of parallel robots via leg observation considering a hidden robot model, Mech. Mach. Theory 106 (2016) 115–147.
[29] Y.-H. Sun, Y. Sun, C.Q. Wu, N. Sepehri, Stability analysis of a controlled mechanical system with parametric uncertainties in Lugre friction model, Int. J. Control 0 (0) (2017) 1–14.
[30] W.-H. Yuan, M.-S. Tsai, A novel approach for forward dynamic analysis of 3-prs parallel manipulator with consideration of friction effect, Robot Comput. Integr. Manuf. 30 (3) (2014) 315–325.
[31] X. Tran, H. Yanada, Dynamic friction behaviors of pneumatic cylinders, Intel. Control Automation 4 (2013) 180–190.
[32] M. Sharifzadeh, A. Arian, A. Salimi Lafmejani, M.T. Masouleh, A. Kalhor, An experimental study on the direct & indirect dynamic identification of an over-constrained 3-dof decoupled parallel mechanism, Mech. Mach. Theory 116 (2017) 178–202.
[33] G. Kothapalli, M.Y. Hassan, Design of a neural network based intelligent pi controller for a pneumatic system, IAENG Int. J. Comput. Sci. 35 (2) (2008) 217–225.
[34] E. Richer, Y. Hurmuzlu, A high performance pneumatic force actuator system: part i nonlinear mathematical model, J. Dyn. Syst. Meas. Control 122 (3) (2000) 416–425.
[35] B. McCarron, Low-Cost IMU Implementation via Sensor Fusion Algorithms in the Arduino Environment, Citeseer, 2013 Ph.D. thesis.
[36] M.B. Thomas, Advanced Servo Control of a Pneumatic Actuator, The Ohio State University, 2003 Ph.D. thesis.
[37] N. Karbasizadeh, M. Zarei, A. Aflakian, M.T. Masouleh, A. Kalhor, Experimental dynamic identification and model feed-forward control of Novint Falcon haptic device, Mechatronics 51 (2018) 19–30.
[38] D. Meng, G. Tao, J. Chen, W. Ban, Modeling of a pneumatic system for high-accuracy position control, Proceedings of International Conference on Fluid Power and Mechatronics, (2011), pp. 505–510.
[39] A. Salimi Lafmejani, B. Danaei, A. Kalhor, M. Tale Masouleh, An experimental study on control of a pneumatic 6-dof Gough-Stewart robot using backstepping-sliding mode and geometry-based quasi-forward kinematic method, Proceedings of the Fifth RSI International Conference on Robotics and Mechatronics (ICRoM), (2017), p. InPress..
[40] H.D. Taghirad, Parallel robots: mechanics and control, CRC press, 2013.